THESIS FOR THE DEGREE OF LICENTIATE OF ENGINEERING

Computational framework for studying charge transport in high-voltage gas-insulated systems

Shailendra Singh

High Voltage Engineering

Department of Material and Manufacturing Technology

CHALMERS UNIVERSITY OF TECHNOLOGY

Gothenburg, Sweden 2015

Computational framework for studying charge transport in high-voltage gas-insulated systems

SHAILENDRA SINGH

High Voltage Engineering

Department of Material and Manufacturing Technology

Chalmers University of Technology

SE-41296 Gothenburg

Sweden

Telephone + 46 (0) 31-772 1000

Computational framework for studying charge transport in high-voltage gas-insulated systems

SHAILENDRA SINGH

Department of Materials and Manufacturing Technology
Chalmers University of Technology

Abstract

Increasing demands in electric energy stimulates a shift in functional requirements to power distribution networks and pushes equipment manufacturers to develop highly optimized products where high rated parameters (e.g., energy, voltages) are combined with reduced geometrical dimensions of components. Thus, newly developed gas-insulated switchgears (GIS) for distribution networks operate at enhanced electric fields which should be withstood by the insulation. In this case, new additional challenges are imposed due to strong requirements concerning environmental safety that call for replacement of SF_6-gas used as insulating medium in GIS by more environmentally friendly substitutes. Ideally, future "green" insulation is to be based on natural gases (e.g. synthetic air), which, however, are characterized by much lower electrical performance and thus need to be strengthen, e.g., by using solid insulating elements. To provide reliable design criteria for hybrid gas-solid insulation, there is a need in detailed understanding of basic physical phenomena taking place due to its exposure to strong electric fields. These include initiation and propagation of electrical discharges in gas phase, interactions of produced gas discharge plasma with solid dielectric surfaces, charge transport though solid material, etc. The research presented in the thesis focuses on analyzing field induced phenomena in gas and aims at developing computer simulation framework incorporating physical processes associated with the motion of charged species in gas medium under electric fields.

The model of electrical discharges in air developed in the present study comprises a set of coupled non-linear partial differential equations (PDE) describing time dependent drift and diffusion of charge carriers associated with reactions between them (ionization, recombination, etc.) ; dynamics of electric fields in discharge volume affected by accumulated space charges; and intensity of photo-ionization in gas. The reactions rate coefficients for the charge transport equations are derived from numerical solution of Boltzmann's equation for electrons energy distribution function in N_2:O_2 (80:20) mixture. The set of PDEs is solved numerically utilizing commercial software based on finite element method. Numerical challenges and details of the implementation are discussed in the thesis; in particular, logarithmic formulation of transport equations, approaches for numerical stabilization of the solution, adaptive mesh refinement, etc. The developed computational framework is utilized for analyzing several study cases including propagation of streamer discharges in air in different 2d geometrical arrangements and streamer branching in fully 3d representation. The obtained results are discussed and compared with results of experimental and theoretical studies available in the literature.

Keywords: high voltage, gaseous dielectrics, gas discharge, low temperature plasma, streamer propagation, drift diffusion equation

Acknowledgments

Shailendra Singh

Göteborg, Sweden

March 2015

iv

Table of Contents

1   Introduction

Electric power distribution networks are undergoing a radical change due to a shift in functional requirements, in particular, increasing distributed power either due to introduction of renewable generation and/or due to growing energy demands from the consumer side. This pushes equipment manufacturers to develop and deliver highly optimized products where high rated parameters (e.g., energy, voltages) are combined with reduced geometrical dimensions of components. The latter, among other consequences, leads to a reduction of insulating distances and, hence, to enhanced electric fields which should be withstood by the insulation. This is typical, for instance, for newly developed gas-insulated switchgears (GIS). In this case, new additional challenges are imposed due to strong requirements concerning environmental safety that call for replacement of SF_6-gas used as insulating medium in GIS by more environmentally friendly substitutes. Ideally, "green" insulation is to be based on natural gases (e.g. synthetic air), which, however, are characterized by much lower electrical performance and thus need to be strengthen, e.g., by using solid insulating elements. To provide reliable design criteria for hybrid gas-solid insulation, there is a need in detailed understanding of basic physical phenomena taking place due to its exposure to strong electric fields. These include initiation and propagation of electrical discharges in gas phase, interactions of produced gas discharge plasma with solid dielectric surfaces (in particular, formation and decay of surface charge layers), polarization and charge transport though solid material, redistribution of electric fields due to accumulated space and surface charges, etc. The research presented in the thesis focuses on analyzing field induced phenomena in gas and aims at developing computer simulation framework incorporating physical process associated with the motion of charged species in gas medium under electric fields.

In gas medium under zero-field conditions, the particles are randomly moving and colliding. The velocities of these particles depend on temperature and density. Moreover, there is a statistical distribution of velocities, which is given by Boltzmann-Maxwell equation [1]

$$\frac{dN_u}{N} = \frac{4}{\sqrt{\pi}} \left(\frac{u}{u_p}\right)^2 \left[e^{-\left(\frac{u}{u_p}\right)^2}\right] \frac{du}{u_p} \tag{1.1}$$

where u is the velocity of a fraction of particles N_u out of total particle density N, u_p is the most probable velocity. A typical velocity distribution is shown in Figure 1.1 [1].

The velocity distribution and the density of particles can be used to calculate the mean free path, which is the distance travelled between collisions

$$\bar{\lambda} = \frac{1}{N\sigma} \tag{1.2}$$

Here, $\bar{\lambda}$ is the mean free path, and σ is the collision cross section. The above equation is simplified representation without considering the motion of target particle.
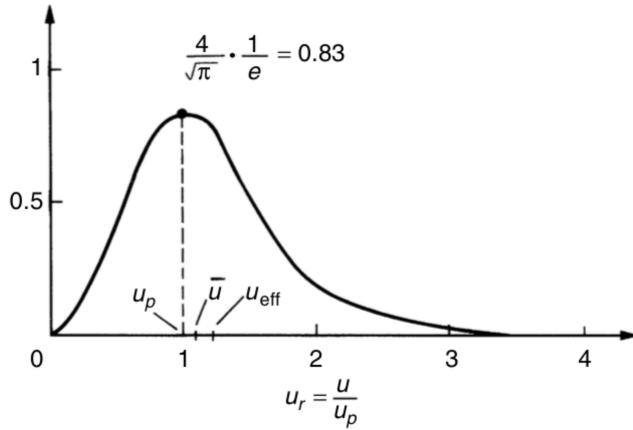
Figure 1.1: Velocity distribution where $\bar{u}$ and u_{eff} are the average and effective velocities, respectively ($\bar{u} = 1.128u_p, u_{eff} = 1.224u_p$)

Collisions among gas particles can be classified as elastic or inelastic. The former case is associated with kinetic energy transfer among the particles while in the latter, a part of kinetic energy is transferred into internal potential energy of the particles-targets. The probability of collisions can be characterized by so-called effective cross sections for the processes. Thus if a fraction of collisions P_i leads, e.g., to ionization, then the effective cross section for ionization is represented by $Q_i = P_i N\sigma$ [1]. The collision frequency for this reaction is $V_e Q_i$ and the reaction rate is $n_e V_e Q_i$, where V_e is the mean electron velocity and n_e is electron density.

Presence of charged species in gas (regardless of their sources) exposed to electric field leads to a great variety of processes due to energy supply from the field to the charge carriers. Thus, collision processes between charged and neutral particles in gas may, in particular, result in [2-5]

- Excitation $e^- + A_2 \rightarrow A_2^* + e^-$

This happens if e.g. an electron e^- with a sufficient energy collides with a gas molecule A_2 in inelastic way that results a transition of the gas molecule to higher vibrational or rotational excited state A_2^*, where it stays for a certain time.

- Electron impact ionization $e^- + A \rightarrow A^+ + 2e^-$

This is the main process of generation of electrons in gas discharges. Thus in air at normal temperature and pressure, approximately 10^3 free electrons are produced in 1 cm^3 due to cosmic radiation and natural radioactivity [6]. Being exposed to an electric field, they accelerate and may gain kinetic energy on their free path high enough to cause ionization of neutral molecule upon impact that results in appearance of new electron and positive ion A^+.

- Electron attachment $e^- + A \rightarrow A^-(+h\nu)$

Some gas atoms or molecules are characterized by so-called electron affinity and can accommodate electrons in their outer electronic shell. Such particles have lower potential energy for negative ion than that of ground state. In case of air, main electronegative components are molecules O_2, CO_2, H_2O. Free electrons in gas can be captured during the attachment process to form negative ions.

- Photoionization $A + h\nu \rightarrow A^+ + e^-$

Being exposed to an electric field, neutral gas molecules can be excited, e.g. by electron impact. As a result of quenching of exited states, photons are produced the energy of which $h\nu$ (h is Planck's constant, ν is the radiation frequency) corresponds to the molecules excitation energy. The photons can be absorbed by nearby molecules leading to their excitation followed by quenching and radiation of photons and so on in a chain manner. Such process is called resonance radiation transport and is typical for discharges in pure gases e.g. nitrogen. In mixtures, the energy of photons released by exited molecules of a certain sort may be higher than the ionization potential of molecules of another type. Hence, absorption of the photon by such particle may lead to its ionization that is indicated by the formula above. This process is typical for air where molecules of oxygen can be ionized by photons released from exited molecules of nitrogen.

- Recombination, e.g., $A^+ + e^- \rightarrow A + h\nu$

This is the process leading to losses of charge carriers in gas. Recombination may take place between positive ions and electrons, as indicated by the formula, or between positive and negative ions if the latter exist in gas as in case of air. The excess energy of the reaction can be transferred to a photon and to a third particle participating in the process.

Such microscopic processes take place in any type of electrical discharges, which in practice are caused by application of a sufficiently high voltage to electrodes immersed in a gas that leads to generation of significant amounts of free charge carriers (electrons and ions) if the applied field exceeds gas ionization threshold. These charged species move along (or opposite, depending upon the charge sign) the direction of the electric field and may eventually cause further ionization forming gas discharge plasma. The magnitude of the applied voltage (to be more precise, the structure and strength of the resulting electric field) decides if the plasma has enough charge generation potential that it can bridge the gap to the ground terminal. The timescale of streamer propagation is in nanoseconds for distance length scale in centimeters. If the voltage is increased further the plasma channel is thermalized and leads to the formation of electrical arc

Plasma associated with electrical discharges is composed of charged species, radicals, excited and ground state species. The types of discharges considered in the present study belong to the class of non-thermal plasmas. This means that the heating effect of background gases can be neglected as the thermal energy provided by the discharge current is not high enough to rise gas temperature and, hence, to enhance plasma production rate. Generally speaking, there is no local thermal equilibrium among particles constituting discharge plasma. Moreover, electrons and other species can have different temperatures and active energy transfer can take place due to the gradient of temperature from electrons to ions and other particles. In general, however, plasmas are quasi-neutral due to conservation principle and various charge generation/dissipation processes ensure that the total charge is conserved.

1.1 Aim and objectives

The general objective of the PhD project is to study physical phenomena associated with the actual processes of migration of charged species in gas-solid high-voltage insulation systems under the influence of strong electric fields. The work focuses on developing a computational framework implementing models of charge transport in gases and on gas-solid interfaces within temporal and spatial scales typical for existing GIS designs. The primary aims are (i) to implement simulation model of gas discharges leading to a dielectric breakdown based on first principle approaches (hydrodynamic model, etc.), and (ii) to introduce solid insulating

elements in form of dielectric barriers and/or coatings to simulate behavior of electrical discharges in hybrid insulation systems.

At the present stage, the thesis focuses on research related to the first aim. The model of discharge processes is formulated in terms of intensities of microscopic reactions (ionization, recombination, electric drift, energy transfer, etc.), which take place between charged and neutral species, and yields macroscopic characteristics such as discharge current, threshold (inception and breakdown) voltages, etc. Simulations with the model are performed for several study cases representing problems of scientific and practical interests and allowing for comparison of calculated and experimental data for verification purposes. In addition, the target of the part of the research related to implementation of the model is to develop an algorithm providing reasonable computational time for practical usage. Such verified and highly efficient model would form a basis of a computational framework which should also allow for further development, e.g., for incorporating solid insulating elements, describing interfacial phenomena (charge trapping/de-trapping on gas-solid interfaces), chemical reactions, heavy species interactions and excited particles interactions as well as thermal effects in the discharge volume.

1.2 Outline of the thesis

The thesis is organized in eight chapters. The first chapter provides introduction and scope of the work. The second chapter presents an overview of gas discharge basics starting from empirical formulations and continuing with introduction of a hydrodynamic model. It also focuses on implementation of the computational model and introduces different quantities (source terms and kinetic coefficients) used in the hydrodynamic model of gas discharge plasma. Issues related to numerical solution of charge transport equations and inherent problems due to their highly non-linear nature and advection dominated flows of charge carriers are tackled in chapter three. Chapter four deals with the solution of the formulated equations in real world applications such as streamers in a needle-plane electrode system and between flat discs. Chapter five presents an extension of the model to 3d space to study streamer branching phenomenon. Chapter six summarizes the accomplished studies. Proposals for future work are formulated in chapter seven.

1.3 List of publications

- M. Ramesh, R. Summer, S. Singh, Y. Serdyuk, S. Gubanski, S. Kumara, Application of streamer criteria for calculations of flashover voltages of gaseous insulation with solid dielectric barrier, Proc. 18th Int. Symp. High Voltage Eng., Aug. 25-30, 2013, Seoul, Korea, pp. 1258-1263.
- S. Singh, Y. Serdyuk, R. Summer, Adaptive numerical simulation of streamer propagation in atmospheric air, Proc. 2013 COMSOL Conference, Rotterdam, the Netherlands
- S. Singh, Y. Serdyuk, R. Summer, S. Gubanski, Simulations of streamers in air using weak-formulation of charge transport equations, J. Phys. D: Appl. Phys., 2015, submitted.
- S. Singh, Y. Serdyuk, R. Summer, Streamer propagation in air in non-axially symmetric electric field, 19th Int. Symp. High Voltage Eng., 2015, Pilsen, Czech Republic, accepted.

- S. Singh, Y. Serdyuk, R. Summer, Streamer branching in air: physical model and simulations in fully 3D spatial domain, Int. Conf. Prop. Appl. of Diel. Materials (ICPADM), 2015, Sydney, Australia, accepted.

Chapter 1 Introduction

2 Overview of gas discharges and modeling approach

Basic facts on studied types of gas discharges as well as modeling approach are presented in this chapter.

2.1 Forms of electrical discharges in gas

When a voltage is applied between a pair of metallic parallel-plate electrodes immersed in air, a current is observed in the external circuit. By varying the applied voltage, the electric field strength between the electrodes can be changed and different processes in gas can be activated resulting in a certain current. Typical discharge voltage-characteristic characteristic for electrodes providing uniform field distribution is shown in Figure 2.1 where different discharge stages are indicated. As seen, the current is extremely weak at low applied voltages and it is due to the drift of charged species existing in gas due to natural background sources (e.g., terrestrial and cosmic radiation, see [7]). Due to the final amount of free charges, this region of the characteristic is linear and obeys Ohm's law. At higher voltages (and fields), all available carriers are participating in charge transport and since their number is not growing (there is always a balance between charge generation and loss processes), the current reaches saturation. At further increasing voltages, the fraction of non-elastic collisions (in their total number) of electrons with neutral molecules increases leading to presence of a large number of exited species and at certain voltage level ionization due to electron impact becomes essential and the current starts growing. This kind of non-self-sustained discharge is called Townsend's discharge after the famous scientist who proposed a theory for this low current regime, which is discussed next.
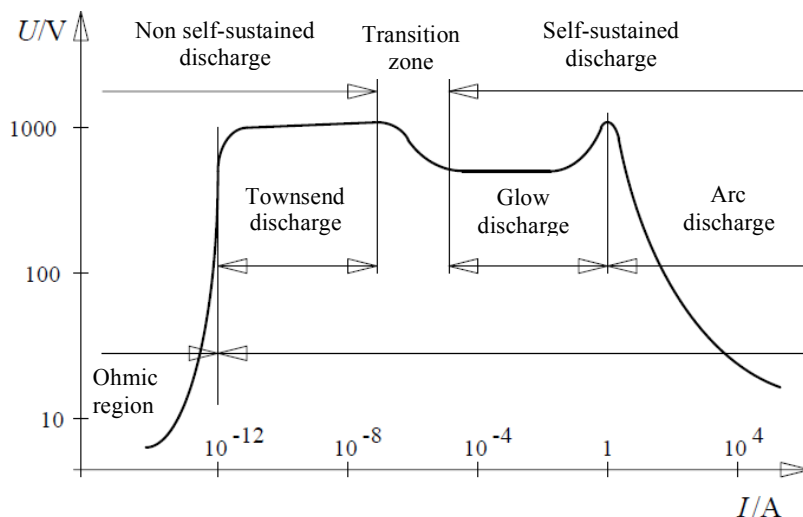

Figure 2.1: Sketch of a current-voltage characteristic of a discharge showing transition between different regimes. Note that voltage-current characteristic is mentioned in the text, here axis (voltage and current) are changed for convenience.

Chapter 2 Overview of gas discharges and modeling approach

2.1.1 Townsend discharge and breakdown

On the rising part of the characteristic corresponding to Townsend's discharge, the electrons gain sufficient energy between collisions to cause impact ionization of gas molecules. The intensity of the impact ionization can be represented by Townsend's first ionization coefficient α [m^{-1}], which is the number of electrons generated by one initial electron due to impact ionization per unit of length of its path in the electric field. Starting with n_0 initial electrons, the total number of electrons after travelling a distance d is $n = n_0 e^{\alpha d}$. This exponential increase in electron numbers $e^{\alpha d}$ is due to the fact that each newly produced electron gains energy from the field and generates new electrons. This process is called electron avalanche in the literature and is shown schematically in Figure 2.2 [1].

The ionization coefficient α is a unique property of gas and depends on electric field strength E and gas pressure p (or density $N = p/kT$, k is Boltzmann's constant, T is gas temperature) and usually is presents as a function of the pressure (density) reduced field E/p (or E/N):

$$\frac{\alpha}{p} = f\left(\frac{E}{p}\right) \tag{2.1}$$

Electronegative gases, as discussed above, are capable to capture free electrons. The strength of this process is characterized by attachment coefficient η [m^{-1}], which is defined in a similar way as Townsend's coefficient by with regards to electron attachment. In practice, the intensity of electrons production in electronegative gases is described by so-called effective ionization coefficient $\bar{\alpha}$ defined as

$$\bar{\alpha} = \alpha - \eta \tag{2.2}$$

At sufficiently high voltages, the production of new electrons and thus positive ions in Townsend's discharge becomes essential and significant amount of ions may reach the cathode. Bombardment of cathode's surface by positive ions leads to a yield of secondary electrons from metal. This process is characterized by Townsend's second coefficient γ, which is a number of electrons released per impact of a single positive ion. Accounting for the secondary electrons, their total number at distance d from the cathode is

$$n = n_0 \frac{e^{\bar{\alpha} d}}{1 - \gamma(e^{\bar{\alpha} d} - 1)} \tag{2.3}$$

The electron yield from the cathode compensates their losses and at certain voltage a transition from Townsend's to a self-sustained discharge takes place. This transition is associated with production of significant space charges and modifications of the electric field in the inter-electrode space in a way that the increased discharge current can be supported by
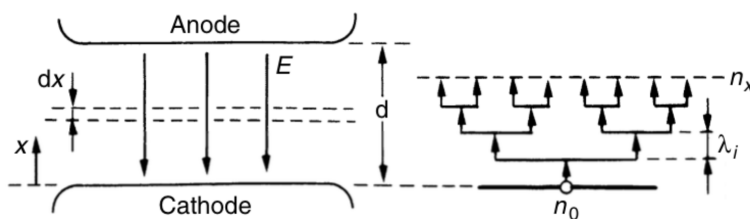

Figure 2.2: Electron multiplication process leading to electron avalanche.

much lower applied voltage. In figure 2.1, this process is indicated as a transition zone and the highest voltage reached on Townsend's discharge branch corresponds is the breakdown voltage. On the right hand side of the transition region, different types of self-sustained discharges occur which belong to classes of glow and arc discharges. These, however, are not subjects of the present study and are not considered further below.

The condition for the breakdown is derived from (2.3) assuming infinite increase in the total number of electrons taking place when the denominator is equal to zero:

$$\bar{\alpha}d = ln\left(\frac{1}{\gamma} + 1\right) \tag{2.4}$$

This expression is known as Townsend's breakdown condition and provides a basis for Paschen's law for breakdown voltages. It states that the electrical breakdown of a gas gap with uniform electric field occurs at a certain voltage which is a function of the product of gas pressure and electrode separation distance as shown in Figure 2.3 for air [1].

The condition (2.4) can be extended to cases with slightly non uniform field by taking $\int \bar{\alpha}\, d\, l$ along the electric field streamline l and comparing it with the magnitude of the right hand side

$$\int_l \bar{\alpha}\, dl = k = ln\left(\frac{1}{\gamma} + 1\right) \tag{2.5}$$

Further extension is possible for cases with strongly divergent fields where even corona discharges may appear, e.g., needle-plane electrode arrangement. In such cases, condition (2.5) requires integration across just a part of the space between electrodes, where ionization takes place, and provides so-called corona inception voltages. For such situations, the value of k to be used in (2.5) has been (and still it is) a subject of discussion, see e.g. [8]. Typically, the value of 9.15 provides a good fit with experimental data for fields ranging from uniform to non-uniform ones [9].

Townsend's theory predicts quite well the breakdown voltages at medium and low gas pressures, small distances and uniform and slightly non-uniform electric fields. When the field non-uniformity increases or distances become large and pressures are higher than several
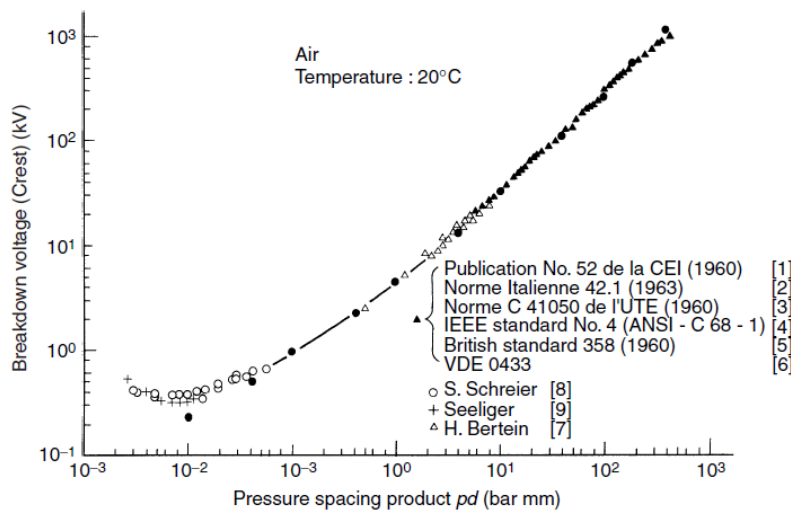

Figure 2.3: Paschen's curve for air taken from [1].

Chapter 2 Overview of gas discharges and modeling approach

2.1.2 Streamer formation and propagation

At high gas pressures (atmospheric and higher) providing values $pd > 10^3$ Torr·cm and sufficiently high voltages, the generated local space charges are strong enough to produce own field which masks the external applied field. This phenomenon can be observed in electrode configurations providing uniform as well as non-uniform field distributions. In the latter case, the ionization of gas starts in a high electric field region and leads to formation of electron avalanches which may attenuate on their way to the counter electrode. If electron avalanches comprising Townsend's discharge are strong and electron generation rate at the tip of a developing electron avalanche is significant, the electric field is enhanced due to the localized space charge in the head and this field may cause a transition of the avalanche to a streamer. For this, the local electric field needs to become comparable with the initial background field that happens when the number of charge carriers (electrons) in the avalanche head becomes larger than ~10^8 (for typical diameter of the head of 100 μm at atmospheric pressure this corresponds to the density ~10^{20} m^{-3} and degree of ionization of the gas ~10^{-5}). A streamer in air is observed as a thin bright channel which is able to propagate even in regions with low fields. Streamer propagation is supported by local processes at its head where the field is extremely high and causes ionization of the gas. Thus, streamer development between electrodes can be seen as a propagation of ionization wave. According to commonly accepted concepts, local generation of charged species at streamer head is associated with photo-ionization of the gas. As discussed above, molecules N_2 excited to higher states by electron impact (typically 1.2-12.65 eV) release photons with energy exceeding ionization potential of molecules O_2 (12.06 eV). The wavelength λ of the emitted light can be estimated as

$$\lambda \leq \frac{ch}{eV} \tag{2.6}$$

where eV is the energy needed for ionization (ionization potential), c is the speed of light and h is Planck's constant. Photoionization leads to "smearing" of streamer head and amplification of charge generation. These processes expand the spatial signature of the moving charge and, as a result, the photoionization maximum appears just in front of the charge edge. It is the source of electrons for the streamer front and leads to enhancement of local electric field due to charge separation between the fast moving electrons and slowly moving ions (note that the mobility of electrons is in 2-3 order of magnitude higher than that of ions thus drift much faster in the gas [1]). The local field strength at streamer head is typically in the range 5-50 MV/m due to small channel radius (10-50 micrometers in air at atmospheric pressure) and high density of charge carriers, which may reach 10^{19}-10^{21} m^{-3}. In this context, streamer development can be seen as propagation of a disturbance in electric field or ionization wave in the gap. One should distinguish between the streamer propagation speed, which is a phase velocity of the ionization wave, and speeds of electrons or ions, which are defined by their mobilities and electric field strength and are essentially velocities of their drift in the field.

Typically, experimental investigations of streamers are conducted utilizing needle-plane, needle-needle or coaxial wire-cylinder configurations, which provide high level of control over streamer development by varying few parameters, like electrodes radiuses, etc. [10]. Voltage-current characteristic are usually recorded during discharge process. In some studies, light emission during streamer development was also recorded with microsecond resolution and very recently in a nanosecond range [11]. Capturing light emission provides a simple way to measure the speed of streamer propagation by way of multiple exposures. The measured propagation speed of streamer head is in the range of 10^7-10^9 m/s [12, 13] and it is dependent on many factors, in particular, electric field distribution between electrodes.

Streamers can be classified according to directions of propagation into positive (cathode directed) and negative (anode directed). The former occurs typically in the vicinity of sharp anode (e.g. needle) where positive space charge appears after single strong or multiple avalanches. This space charge generates a field, which screens out the external field at the anode and produces a spike in front of the space charge cloud, where photoionization starts providing conditions for streamer inception. In case of negative streamers, avalanches can reach critical number of charge carriers on their way from the cathode to the anode and streamer channel can grow due to secondary avalanches produced by runaway electrons (thus, there is no need in photoionization). Further progression of streamers in gas requires certain minimal field strength, which is called propagation field in the literature. Thus, the background electric field needed for positive streamer is in the range of 0.4-0.6 MV/m whereas for negative streamer it is in the range 1-2 MV/m [1]. The difference in the propagation field is due to various secondary mechanisms supporting discharge development as mentioned above.

If field pattern is characterized by enhancements at both electrodes (e.g., needle-needle or sphere-sphere systems), the streamer propagation can be bidirectional. In such case, streamers heads are created at locations of strong fields at both the anode and the cathode and discharge channels from both sides of the gap propagate towards each other and eventually meet in the bulk of the gas volume. An example of such situation is considered below as a study case.

2.2 Streamer modeling

Physical processes in non-thermal gas discharges are usually modeled utilizing kinetic, hydrodynamic or hybrid approaches [14-17]. The second one is the most popular for types of discharges dealt with in the thesis and, therefore, it is presented in details below.

2.2.1 Drift-diffusion equations for charge carriers

Within a hydrodynamic approximation, dynamic behavior of charge carriers in gas is considered as a motion of corresponding fluids (electronic and ionic), which are characterized by volume densities of the carriers n [m^{-3}] and are controlled by electrostatic forces. The latter define convective fluxes of charged species $n\mathbf{w}$ [m^{-2}s^{-1}] associated with their drift velocities $\mathbf{w}$ [m/s]. In addition, diffusive fluxes may exist due to gradients of carriers' densities ∇n. The concentrations of the charged particles may change locally due to different mechanisms of their generation and loss, rates of which R [m^{-3}s^{-1}] are typically dependent of the intensity of the local electric field. All these result in time variations of the densities of electrons and ions that can be described by respective mass conservation equations also known as continuity equations for corresponding fluxes. In case of air, the set of PDEs can be written as follows reducing consideration of ionic species in gas to two generic types of ions (positive and negative)

$$\frac{\partial n_e}{\partial t} + \nabla \cdot (-n_e \mathbf{w}_e - D_e \nabla n_e) = R_e$$

$$\frac{\partial n_p}{\partial t} + \nabla \cdot (-n_p \mathbf{w}_p - D_p \nabla n_p) = R_p \qquad (2.7)$$

$$\frac{\partial n_n}{\partial t} + \nabla \cdot (-n_n \mathbf{w}_n - D_n \nabla n_n) = R_n$$

Here, subscripts e, p and n indicate electrons, positive and negative ions, respectively; D stands for diffusion coefficient. The source terms in (2.7) incorporate rates of processes to be considered in the model. Typical set of reactions includes electron impact ionization and

attachment, recombination of charge carriers as well as background ionization and photoionization of the gas. The resulting rates of the processes for the different charged particles can be expressed as

$$R_e = \alpha\, n_e|w_e| - \eta\, n_e|w_e| - \beta_{ep}n_en_p + R_0 + R_{ph}$$

$$R_p = \alpha\, n_e|w_e| - \beta_{ep}n_en_p - \beta_{pn}n_pn_n + R_0 + R_{ph} \qquad (2.8)$$

$$R_n = \eta\, n_e|w_e| - \beta_{pn}n_pn_n$$

where β_{ep} and β_{pn} are coefficients of electron-ion and ion-ion recombination $[m^3 s^{-1}]$, respectively; R_0 and R_{ph} are the rates of background and photo ionization, $[m^{-3}s^{-1}]$, respectively. Note that positive sign in (2.8) indicates sources of the charged species while negative sign indicates rates of losses.

Since most of the parameters in (2.7) and (2.8) are dependent on the electric field **E**, the drift diffusion equations are to be coupled with Poisson's equation

$$\nabla(-\epsilon_0\epsilon_r \nabla V) = e\,(n_p - n_e - n_n) \qquad (2.9)$$

$$-\nabla V = \mathbf{E} \qquad (2.10)$$

Here, ϵ_0 is the permittivity of vacuum, ϵ_r is the relative permittivity, V is the electric potential and e is electron charge. Note that the right hand side of Poisson's equation comprises the volume charge density, which varies in space occupied by the discharge and may lead to local field enhancements or weakening thus affecting different volumetric sources/sinks of charged species and their fluxes. Thus, equations (2.7)-(2.10) are coupled via field dependencies of the problem parameters.

2.3 Calculations of kinetic coefficients

Parameters and rate coefficients in the hydrodynamic models can be obtained from a solution of Boltzmann's equation, which can be written in phase space for a distribution function $f(\mathbf{v}, \mathbf{r})$ such that the scalar quantities (e.g. number density) can be evaluated as moments of the solution. The general form of Boltzmann's equation is written as

$$\frac{Df}{Dt} = J_{st}(f), \quad \text{where} \quad \frac{D}{Dt} = \frac{\partial}{\partial t} + \mathbf{v}\frac{\partial}{\partial \mathbf{r}} + \mathbf{F}\frac{\partial}{\partial \mathbf{v}} \qquad (2.11)$$

Here variables **v** and **r** in (3.5) represent the velocity and position vector of a particle, respectively, and J_{st} is the collision integral [18]. According to (2.11), the total time variance of the distribution function is due to the sum of rates of its changes due to an external force **F**, diffusion and collisions. The equation for charged species (e.g. electrons) can be written accounting for the external electrostatic force provided by the electric field.

As seen, the energy distribution function is defined by six dimensions in phase space (space vector **r** and velocity vector **v**). In order to reduce the complexity, assumptions are usually made, in particular, using symmetry of electron distribution in momentum/velocity space, the equation can be reduced to four dimensions including time co-ordinate. Further simplifications, e.g. by utilizing spherical harmonics expansion, yield the following equation for the isotropic part of the distribution function f_0 and anisotropic part f_1 [19].

This means that out of three-position vector, the distribution function is only dependent on one space variable z:

$$\frac{\partial f_0}{\partial t} + \frac{\Upsilon}{3} \varepsilon^{1/2} \frac{\partial f_1}{\partial z} - \frac{\Upsilon}{3} \varepsilon^{-1/2} \frac{\partial f_1}{\partial \varepsilon} \varepsilon \mathbf{E} f_1 = C_0$$

$$\frac{\partial f_1}{\partial t} + \Upsilon \varepsilon^{1/2} \frac{\partial f_0}{\partial z} - \mathbf{E} \Upsilon \varepsilon^{\frac{1}{2}} \frac{\partial f_0}{\partial \varepsilon} = -N \sigma_m \Upsilon \varepsilon^{1/2} f_1$$

(2.12)

Here, Υ is a constant defined as $(2e/m_e)^{1/2}$; C_0 is the collision generation rate for f_0; ε and $\mathbf{E}$ stand for the electron energy and electric field, respectively. It is further assumed that there is no time varying contribution to the isotropic part f_0. Accounting for this, f_0 can be reduced to F_0, which is obtained from equation (2.13):

$$\frac{\partial}{\partial \varepsilon}\left(\widetilde{W} F_0 - \widetilde{D} \frac{\partial F_0}{\partial \varepsilon}\right) = \widetilde{S}$$

(2.13)

where $\widetilde{W}$ represents velocity associated with negative energy flux (cooling by collisions with neutrals and electrons with lower energy); $\widetilde{D}$ stands for the heating by high energy species. Note that $\widetilde{W}$ and $\widetilde{D}$ reprents the elastic collisions associated with electron energy distribution function (EEDF) whereas $\widetilde{S}$ is the source assocsiated with the inelastic collisions processes discussed earlier [19-21].

Knowing F_0, the electron density is obtained by integrating it over velocity space

$$n_e = 4\pi \int_0^\infty F_0\, v^2 dv$$

(2.14)

In general, the mass conservation (drift-diffusion) equations (2.7) can be deduced from (2.13) by multiplying it with $\varepsilon^{1/2}$ and integrating over all energies:

$$\frac{\partial n_e}{\partial t} + \frac{\partial\left(-\mu \mathbf{E} n_e - \frac{\partial D_e n_e}{\partial z}\right)}{\partial z} = C_0$$

(2.15)

where μ is the mobility and D is diffusion coefficient found as

$$\mu_e N = \frac{\Upsilon}{3} \int_0^\infty \frac{\varepsilon}{\sigma_m} \frac{\partial F_0}{\partial \varepsilon} d\varepsilon$$

(2.16)

$$D_e N = \frac{\Upsilon}{3} \int_0^\infty \frac{\varepsilon}{\sigma_m} F_0 d\varepsilon$$

(2.17)

where σ_m is effective cross-section for all collision processes.

The coefficients needed for setting up the drift-diffusion equations for synthetic air (mixture 80% nitrogen and 20% oxygen) are obtained from the solution of Boltzmann's equation for the mixture. Thus, by knowing the electrons energy distribution function, effective rates of ionization, attachment, and recombination can be evaluated. In the present study, Boltzmann's equation is solved using two-term approximation (isotropic-anisotropic part, as explained above) for the regime in which a small fraction of collisions are inelastic. The solution is found by utilizing Galerkin method as implemented in COMSOL Multiphysics Plasma module [22]. The collisions considered in the calculations include those leading to excitation and ionization of molecules by electron impact and electron attachment [19]

$$\widetilde{S} = \left(\sum_k C_k\right)$$

(2.18)

Here, C_k indicates all types of collisions causing energy exchange as described in chapter 1, which are functions of electron energy and cross section. Since equation (2.13) is a one-dimensional partial differential equation of convective-diffusive type with respect to energy, it is solved by discretizing over electron energy with following boundary conditions.

$$F_0 = 0 \ at \ \varepsilon = \ \infty \tag{2.19}$$

$$\frac{\partial F_0}{\partial \varepsilon} = 0 \ at \ \varepsilon = \ 0 \tag{2.20}$$

In the calculations, the highest value of electrons energy is taken to be high enough that it encompasses all the reactions, e.g. $\varepsilon = 100$.

The source terms in the drift-diffusion equations (2.7) are defined in terms of reactions rates and solution of Boltzmann's equation yields rate coefficients as function of electron energy for the collisions (2.18). Thus, the rate coefficient k_k for k_{th} collision process is defined by [21]

$$k_k = \ \gamma \ \int_0^\infty \varepsilon \ \sigma_k F_0 d\varepsilon \tag{2.21}$$

where σ_k is the corresponding cross-section. In the present calculations, the cross-section data for interactions of electrons with molecules of N_2 and O_2 were taken from databases [23] and [21].

Knowing the coefficient k_k, the reaction rate R_k is obtained as

$$R_k = \ k_k x_k N \ n_e \tag{2.22}$$

where x_k is the mole fraction of target species and N is the gas density. Considering (2.22) to be applied to electron impact ionization of neutral species (with corresponding cross-section), one may link Townsend's ionization coefficient to the rate coefficient [19]

$$\frac{\alpha_k}{N} = \frac{k_k}{\mu_e E} \tag{2.23}$$

The outcome from the calculations is the rates of reactions as functions of a reduced electric field (ration E/N) for the mixture N_2:O_2 (80:20). To be used in equations (2.7)-(2.8), the reaction rates are converted into Townsend's ionization coefficient and attachment coefficient according to [19]. To verify the results, they are compared with those obtained using popular Boltzmann equation solver BOLSIG+ [19, 23] in Figures 2.4-2.7. It can be seen that there is very good match between both sets of results for pure gases as well as for the mixture. Threshold values of the reduced electric field can be identified for field dependences of the ionization coefficients above which the curves show an exponential increase. Note that the attachment rates of electrons to molecules O_2 are calculated for two-body collisions. .

The results of the calculations of the ionization and attachment coefficients for the mixture are compared with the experimental results for air [24, 25] in Figures 2.8 and 2.9, respectively. The achieved agreement confirms the validity of the theoretical results, which were utilized in the simulations of discharges presented in the following chapters.

Transport coefficients needed for simulations of discharges were obtained from available empirical data. Thus, field dependences of the drift velocity [12, 13, 26, 27] and diffusion coefficient [12, 28] of electrons in air are often approximated as a power functions of the reduced field, which matches with equations (2.16-2.17):

$$\mathbf{w_e} = 3.2 \text{ x } 10^3 \left(\frac{E}{N}\right)^{0.8} \text{m/s} \tag{2.24}$$

$$D_e = 7 \times 10^{-2} + 8 \times \left(\frac{E}{N}\right)^{0.8}, \text{m}^2/\text{s} \tag{2.25}$$

Magnitudes of other parameters used in the model are presented in Table 2.1 [12, 13, 26-29]. Different approximations used by various authors for swarm parameters can be found elsewhere [30].
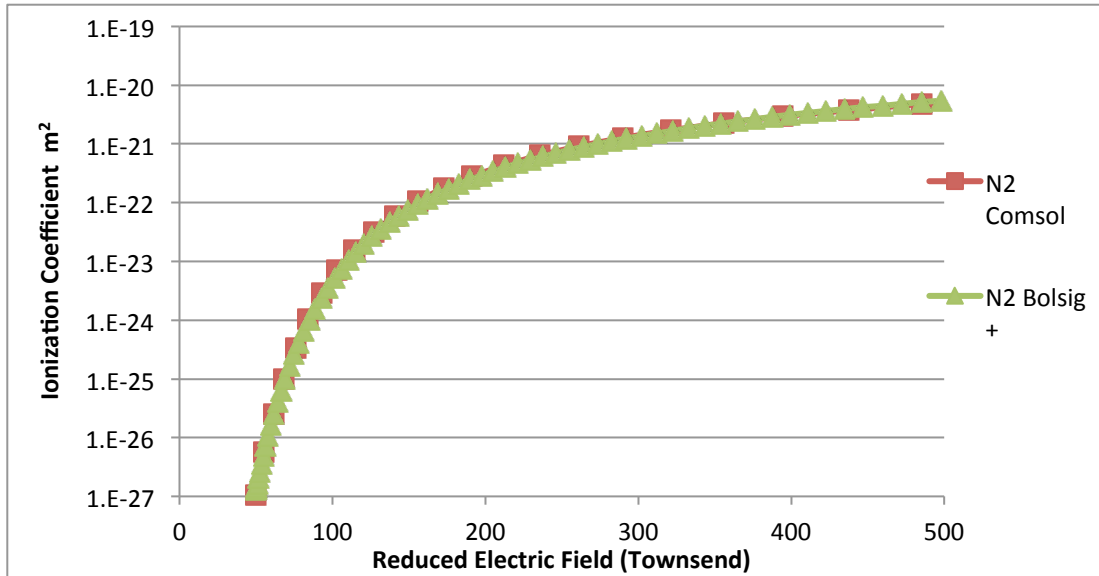

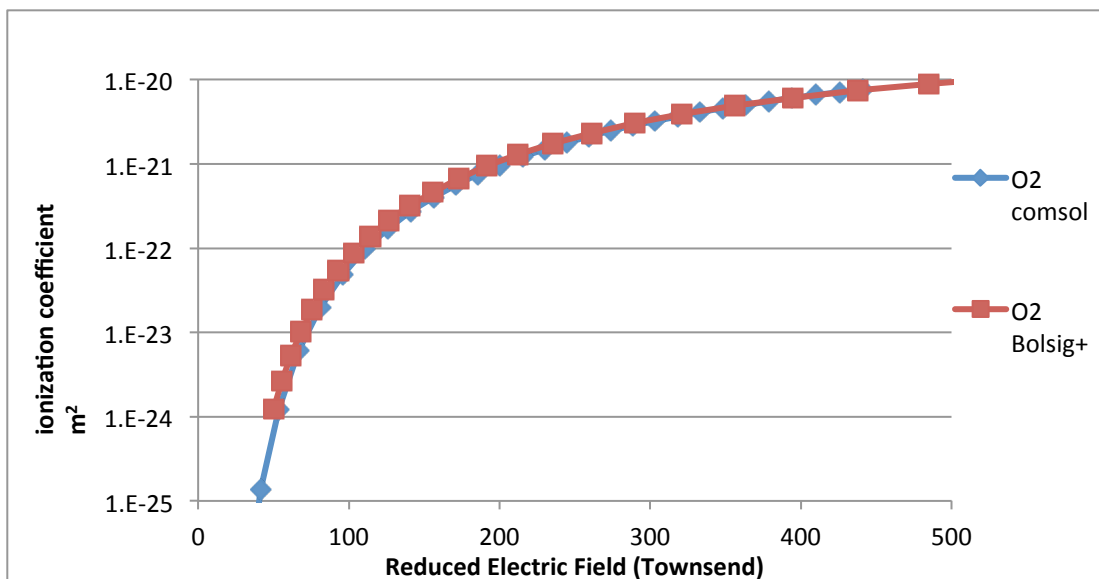Figure 2.4: Ionization coefficient in N2 vs. reduced electric field

Figure 2.5: Ionization coefficient in O2 vs. reduced electric field
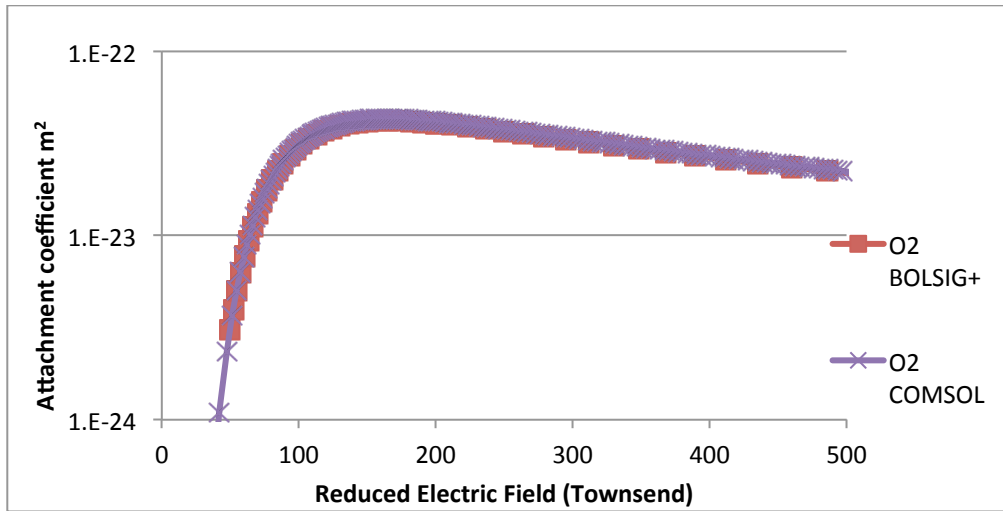
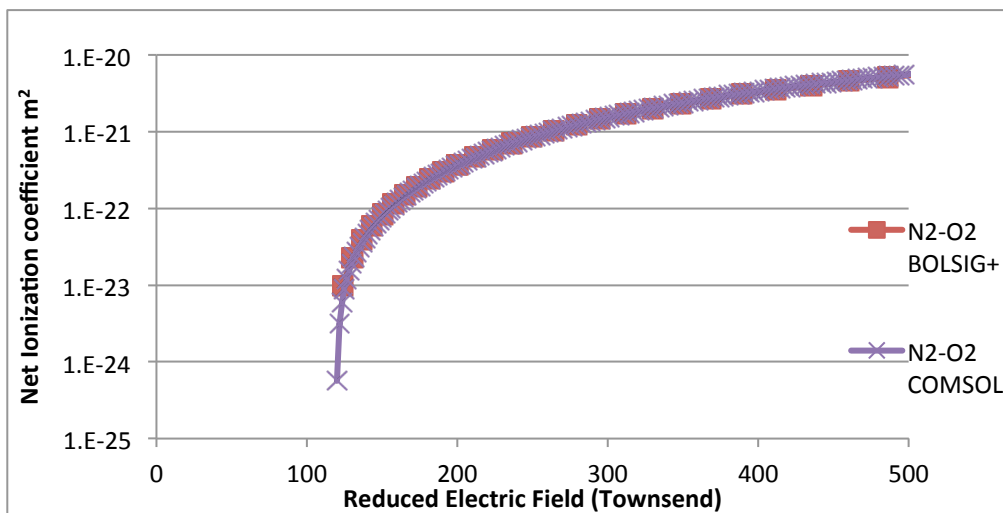Figure 2.6: Attachment coefficient in O2 vs. reduced electric field

Figure 2.7: Net ionization coefficient of air vs. reduced electric field
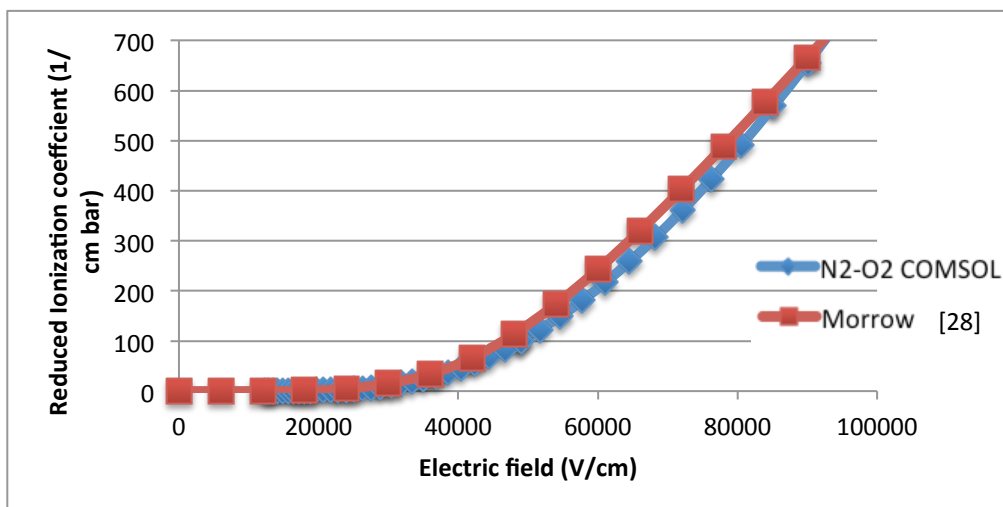

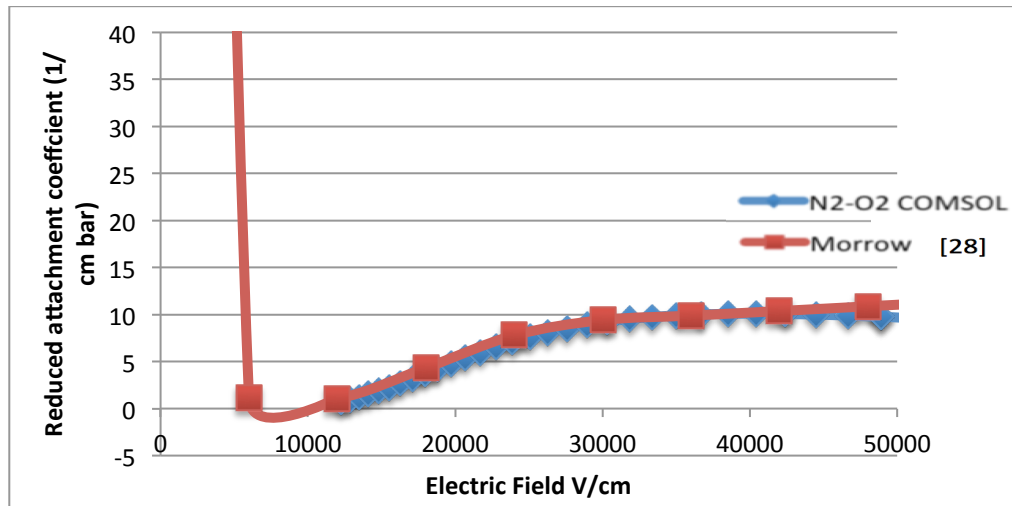Figure 2.8: Ionization coefficient of air (calculated vs. empirical data)

Figure 2.9: Attachment coefficient for air as a function of the Electric field.

Table 2.1: Parameters used in the simulations

Parameter	Magnitude	Definition
μ_p m^2/Vs	2e-4	mobility of positive ions
D_p m^2/s	5.05e-6	diffusion coefficient of positive ions
μ_n m^2/Vs	2.2e-4	mobility of negative ions
D_n m^2/s	5.56e-6	diffusion coefficient of negative ions
β_{ep} m^3/s	5e-4	recombination rate of electron and positive ions
β_{pn} m^3/s	2.07e-12	recombination rate of positive and negative ions
R_0 1/m^{3}s	1.7e9	background ionization rate
k_{det} m^3/s	1e-18	electron detachment rate

Note that the swarm parameters and rate coefficients described above are valid only when the reduced electric field E/N is relatively weak (<500 Townsends) allowing for distribution function to be considered as isotropic [31].

2.4 Photoionization

The additional source included in the drift diffusion equation is photo-ionization, which is a non-local source of seed electrons in front of streamer head during streamer propagation. For simulations purposes, it is possible to replicate the effect of photoionization by introducing reasonably high background density of electrons that has been implemented in several studies, e.g. [32-34]. However, such approach is not physically meaningful and, therefore, models of photoionization in gas discharges in air have been introduced.

According to the existing theories [33, 35], photons in air appear due to quenching of excited nitrogen molecules to ground stage and they transfer energy (1.2 -12.65) eV sufficient for ionization of oxygen molecules with the ionization potential 12.06 eV:

$$e^- + N_2 \rightarrow e^- + N_2^*$$

$$N_2^* \rightarrow N_2 + h\nu_{UV} \tag{2.26}$$

$$O_2 + h\nu_{UV} \rightarrow e^- + O_2^+$$

The frequency interval considered for UV photons $h\nu_{UV}$ in air radiated by excited nitrogen molecules is 98 – 102.5 nm.

Early streamer models were based on integral formulation of photoionization process [36]. The principle used was based on considering the local photoionization rate at a given point as a sum of contributions from all photons born in the gas and travelling through it, which are being absorbed at this location with a certain probability. The latter is characterized by an absorption coefficient. It can be seen like ray tracing in which individual UV rays are generated from each element to the observation point with certain attenuation based on geometric length or view factor.

The integral form of the ionization rate can be written as [34, 36]

$$R_{ph}(\mathbf{r}, t) = c \int_0^\infty dv\, \kappa \int_\Omega \Psi\, d\Omega \tag{2.27}$$

where $\Psi(\mathbf{r}, \mathbf{\Omega}, t)$ is radiative distribution function for a given frequency ν, position vector $\mathbf{r}$, direction $\mathbf{\Omega}$ (solid angle) and time t; κ is photoionization coefficient defined by the product of photoionization efficiency [32] and absorption coefficient; c is the speed of light.

Zhelzenayak et al [36] proposed an integration procedure over entire discharge volume for obtaining the photoionization source. The integration is to be applied to the product of photon generation rate $I(\mathbf{r})$ and function $g(R)$, which is a radiation absorption function. In the following, R denotes the magnitude of the difference between the observation position vector and a vector defining other position contributing to photoionization. Since the number density of excited molecules in gas is related to the impact ionization intensity, photon production rate $I(\mathbf{r})$ is assumed to be proportional to the ionization rate. Accounting for this, the rate of photoionization is written as

$$R_{ph}(r) = \iiint \frac{I(r)g(R)}{4\pi R^2}\, dV \tag{2.28}$$

This equation can be derived from the transport equation of radiation distribution function $\Psi(\mathbf{r}, \mathbf{\Omega}, \mathbf{t})$

$$\frac{\partial \Psi}{\partial t} + c\, \mathbf{\Omega}\, \nabla\, \Psi = \sum_{u,d} \frac{n_u \emptyset_{ud}}{4\pi\, \tau_{ud}} - \kappa_\nu\, c\, \Psi \tag{2.29}$$

where subscripts u and d represent energy levels of excited species and summation is done over all u such that $d < u$; κ_ν is the absorption coefficient and $1/\tau_{ud}$ represents Einstein's coefficient for spontaneous transition; n_u is the number density of excited species at level u; $\emptyset_{ud}$ is normalizing function.

Assuming instantaneous emission of photons, one can obtain

$$R_{ph}(r, t) = \iiint \frac{n_u(r't) * \emptyset_u}{4\pi R^2 c\, \tau_u} \exp(-\kappa_\nu R)\, dV' \tag{2.30}$$

The photon absorption coefficient within the considered frequency range is introduced as

$$\kappa_v = \kappa_1 \left(\frac{\kappa_2}{\kappa_1}\right)^{(\kappa_v - \kappa_1)/(\kappa_2 - \kappa_1)} \tag{2.31}$$

Here, κ_1 and κ_2 are the values corresponding to the minimum and maximum frequencies, respectively. The absorption coefficient is approximated in [36] as a function of partial pressure of oxygen p_{O_2} in air

$$\kappa_1 = .035 p_{O_2} \quad \text{and} \quad \kappa_2 = 2\, p_{O_2} \tag{2.32}$$

This yields the absorption function in the form

$$\frac{g(R)}{p_{O_2}} = \frac{\exp(-\kappa_1 R) - \exp(-\kappa_2 R)}{p_{O_2} R \ln\left(\frac{\kappa_2}{\kappa_1}\right)} \tag{2.33}$$

After introducing into (2.28), the solution of the resulting equation is to be updated for each time step while solving the set of PDEs describing evolution of gas discharge plasma. This makes the solution time for the whole problem using this type of integral formulation to be unacceptably long. In addition, the demands to the hardware (in particular computer RAM) are extremely high since the integration is needed for each point in the discharge volume accounting for contributions from all the other points that results in a full matrix to be stored. Several strategies were devised over the years to overcome the problem. Thus, Kulikovsky [32, 37, 38] proposed a system of rings as emitting source for axisymmetric geometry and the contribution from each ring to the source point was calculated by the use of a geometric factor calculated once and stored. Other strategies included use of a fine grid near streamer head and coarse grid everywhere else in the discharge volume to reduce the integration efforts [34, 39].

The direct numerical solution for obtaining the photoionization rate employs Eddington method [40]. Another method developed by Lowke et al. [2] and Bourdon et al. [34], does not include direct numerical solution but starts at equation (2.28) proposed by Zhelzenayak. Further, the $g(R)/R$ function is replaced by a series of exponential functions. These yield integral terms R_{ph}^n

$$R_{ph}(\mathbf{r}) = \sum_n R_{ph}^n(\mathbf{r}) \tag{2.34}$$

$$R_{ph}^n(\mathbf{r}) = \iiint \frac{I(\mathbf{r}')A_n p_{O_2}^2 \exp(-\lambda_n p_{O_2} R)}{4\pi R} dV' \tag{2.35}$$

which are assumed to be solutions of Helmholtz equations

$$\nabla^2 R_{ph}^n(\mathbf{r}) - \left(\lambda_n p_{O_2}\right)^2 R_{ph}^n(\mathbf{r}) = -A_n p_{O_2}^2\, I(\mathbf{r}) \tag{2.35}$$

In the present study, three terms are accounted for the summation (2.37). Hence, the resulting set Helmholtz equations to be solved is

$$\nabla^2 R_{ph}^1 - \left(\lambda_1 p_{O_2}\right)^2 R_{ph}^1 = -A_1 p_{O_2}^2\, I$$
$$\nabla^2 R_{ph}^2 - \left(\lambda_2 p_{O_2}\right)^2 R_{ph}^2 = -A_2 p_{O_2}^2\, I \tag{2.36}$$
$$\nabla^2 R_{ph}^3 - \left(\lambda_3 p_{O_2}\right)^2 R_{ph}^3 = -A_3 p_{O_2}^2\, I$$

Table: 2.2: fitting parameters used in (2.36)

n	A_n, (cm Torr)$^{-2}$	λ_n, (cm Torr)$^{-1}$
1	1.986e-4	.0553
2	.0051	.146
3	.4886	.89

and finally the photoionization rate is

$$R_{ph} = R_{ph}^1 + R_{ph}^2 + R_{ph}^3 \tag{2.37}$$

Here, A_n and λ_n are fitting parameters taken from [34] (shown in Table 3.2); I is the photon generation intensity proportional to the ionization rate. It has been proven in [34] that three term approximation provides better fit to the integral model than the two term approximation and yields closer match to Eddington direct solutions [34, 40].

3   Numerical Implementation

The drift-diffusion equations for fluxes of charged species together with Helmholtz and Poisson equations (for photoionization rate and electric potential, respectively) are solved in COMSOL Multiphysics. The mathematical module is used to set up the equations that allowed for writing custom weak formulation to obtain numerical solution. For this, the drift-diffusion equations are modified as described below to get a stable numerical solution.

3.1   Logarithmic formulation of transport equations

As indicated in the previous chapter, the hydrodynamic approximation used to describe transport of charge carries in discharge plasma utilizes drift-diffusion equations with source/sinks terms determined by different microscopic processes. The PDEs are to be solved numerically due to strong couplings, non-linearity and field dependent coefficients involved. Numerical solution assumes that the equation is discretized on a computational mesh using certain procedure, e.g. utilizing finite elements (FE) method for which the original equation is transformed into so-called weak form that is essentially an integral form of the PDE.

The most challenging part in the numerical solution of the streamer model equations consist in resolving transport equations for the changes species, in particular electrons. Let us consider a convection-diffusion equation, where u is a scalar quantity like a number density

$$\frac{\partial u}{\partial t} + \nabla u(\boldsymbol{\beta} - D\,\nabla u) = source \tag{3.1}$$

Assuming for simplicity one-dimensional case (x is the co-ordinate) and constant velocity $\boldsymbol{\beta}$ and diffusion coefficient D, expanding the brackets yields

$$\frac{\partial u}{\partial t} + \nabla u \boldsymbol{\beta} - D\,\Delta u = source \tag{3.2}$$

A solution can be derived using, e.g., so-called method of characteristics based on known pattern of particles streamlines. The idea here is to reduce the PDE to ordinary differential equation (ODE) such that the scalar quantity along a streamline is dependent on only one space coordinate i.e. streamline curve length. The streamlines are defined by a family of curves $\boldsymbol{x}$ such that

$$\frac{dx_i}{ds} = \beta_i \tag{3.3}$$

where 's' is a parameter. This approach, however, does not allow to overcome issues, first of all stability and positivity of the solution, related to the nature of (3.1) while applying it to charge transport in streamers. Thus, the second and the third terms in the equation are convective flux u$\boldsymbol{\beta}$ and diffusive flux $D\nabla u$, respectively. If the problem is dominated by diffusion, the FE formulation is stable [41]. In case when diffusive flux is small as compared to convective flux, the PDE is essentially of hyperbolic type and its numerical solution obtained with conventional algorithms is inherently unstable exhibiting oscillations like those
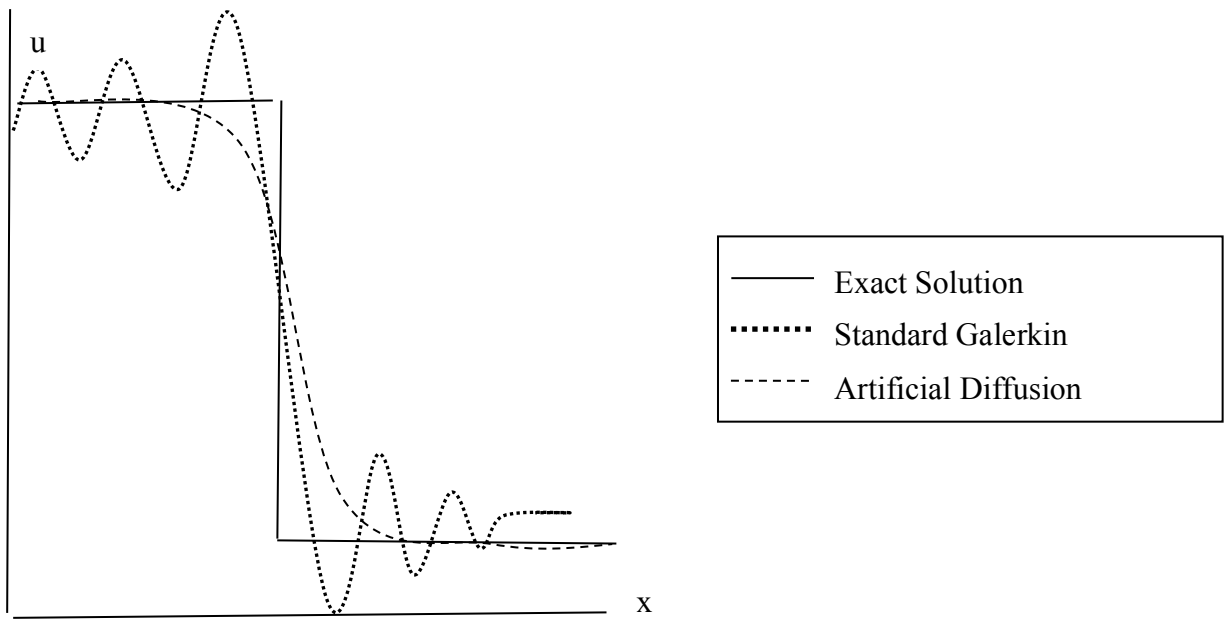
Figure 3.1: Solution of a steady state convection–diffusion equation at discontinuity

in Figure 3.1. The stability conditions are usually linked to so-called Peclet number for a given mesh size *h*

$$Pe = \frac{|\beta|h}{2D} \tag{3.4}$$

which indicates relative contributions of convective flux and diffusive fluxes. If Peclet number is greater than unity, that is typical for streamer propagation problem, oscillations in the solution appear. The higher is the value of *Pe* the stronger instability occurs which may lead to even unphysical results such as negative concentrations of charge carriers. Preventing these effects requires implementing special approaches since the positivity of the solution of (3.1) is not guaranteed by FE formulation, as the shape function is not obeying conservation principle. Various methods to tackle this problem have been proposed, e.g., introducing artificial source terms, which provide positive carriers density when it becomes too low. Also, neglecting the negative densities and replacing them with some small positive magnitudes is sometimes used. Such methods, however, are fully artificial and are not based on any physical background.

A consistent way of avoiding numerical artifacts in the solution is to formulate original drift-diffusion equations in equivalent logarithmic form so that the problem is to be solved for the log of the number density. Such formulation ensures that the concentration of species always remains positive without the need in an artificial source or density capping. This also helps when the gradients in the solution are strong like in case of streamer head, where the number density of electrons may change in 10 orders of magnitude over few mesh elements. The drawback of this approach, however, is the fact that the non-linearity of the problem becomes much stronger.

The transformation of the original equations (3.1) is done by introducing new variables $nel = \ln(n_e)$, $npl = \ln(n_p)$, $nnl = \ln(n_n)$. Reconsidering all terms, this yields

$$\exp{(nel)}\frac{\partial nel}{\partial t} + \nabla.\left(-\exp{(nel)}\mathbf{w}_e - D_e\exp{(nel)}\nabla\ nel\right) =\ R_e$$

$$\exp{(npl)}\frac{\partial npl}{\partial t} + \nabla.\left(-\exp{(npl)}\mathbf{w}_e - D_e\exp{(npl)}\nabla\ npl\right) =\ R_p \qquad\qquad (3.5)$$

$$\exp{(nnl)}\frac{\partial nnl}{\partial t} + \nabla.\left(-\exp{(nnl)}\mathbf{w}_e - D_e\exp{(nnl)}\nabla\ nnl\right) =\ R_n$$

These modified equations are valid for any co-ordinate system (like the original ones) and boundary conditions are to be written in logarithmic form too.

3.2 Stabilization techniques

Solving equations (3.5) written in logarithmic form still is challenging task. Even if the positivity of the solution is preserved oscillations similar to those in Figure 3.1 may appear. A traditional way of damping them is to introduce some artificial diffusion to the original equation that, in turn, may lead to inaccuracies in the solution. Numerical stabilization techniques can be classified as isotropic diffusion, streamline diffusion and crosswind diffusion. The simplest approach is realized within the first method: an extra diffusion is added to the diffusion coefficient such that Peclet number becomes less than unity

$$Pe =\ \frac{|\beta|h}{2\,(D+D_{iso})} \qquad\qquad (3.6)$$

While doing so, the original problem is affected yielding more diffusive solution. That is the reason this method is often referred to as inconsistent stabilization.

Selective artificial diffusion can be also introduced in such a way that the resulted equation remains consistent with the original formulation. Such consistent stabilization can be implemented in different ways, e.g. utilizing so-called streamline diffusion [41]. This method selectively introduces diffusion along streamline direction only. Moreover, Galerkin FE formulation can be modified by introducing a trial function dependent on flow direction and this new trial function yields same solution as for the original equation [41]. This streamline diffusion method is also known as streamline upwind Petrov-Galerkin method (SUPG). It can be further advanced by introducing so-called shock capturing technique (require modifying test function for both streamline and crosswind directions) known as crosswind diffusion. Both trial functions based on these methods are consistent with original formulation.

In COMSOL Multiphysics package, both consistent and inconsistent types of stabilization are provided for general problems. When using the former, the numerical solution is forced to converge to an exact solution for the cost of increased non-linearity (and thus increased total size of the problem and reduced convergence rate) whereas the latter method redefines the original problem increasing artificially the diffusive term. In general, the inconsistent stabilization with isotropic diffusion is more robust and yields faster convergence, but sharp gradients in the solution are smeared out due to the increased diffusion term.

In the present study, consistent SUPG stabilization is introduced through weak formulation in general mathematics module of COMSOL Multiphysics. It was verified by using standard 1d test case for drift-diffusion equations with sharp gradients as described in the following section.

3.3   Numerical test of stabilization in 1d test case

A 1d problem is defined for scalar quantity 'u' which represents particles concentration. To make the case even more complex, pure convection is considered as it makes the whole system unstable due to the lack of diffusion and a nonlinear source term is added to the right hand side:

$$\frac{\partial u}{\partial t} + 2\frac{\partial u}{\partial x} = -u(u-1)(u-0.5) \tag{3.7}$$

The logarithmic formulation is achieved by introducing new variable $ul = \log(ul)$:

$$\frac{\partial \exp(ul)}{\partial t} + 2\frac{\partial \exp(ul)}{\partial x} = -\exp(ul)(\exp(ul)-1)(\exp(ul)-0.5) \tag{3.8}$$

A periodic boundary condition is used such that the outlet flux is taken as inlet flux. A uniform 1d mesh is used to discretize the spatial domain. The initial condition for the unknown variable is a rectangular pulse as shown in Figures 3.2 – 3.4 together with the profiles obtained after certain period of time (indicated in the legends).

As seen, the solution of the original equation (3.7) shown in Figure 3.2 suffers from strong oscillations and it becomes negative on the tail of the pulse. Positivity is preserved in the solution obtained with the logarithmic formulation (3.8), as shown in Figure 3.3, while the oscillations are even stronger than in the previous case. To avoid the perturbations, stabilization is introduced in the form of variations in the test function with gradients of the primary variable. This approach prevents changing the nature of the formulation that is not the case with artificial diffusion[41]. To realize such stabilization, an additional source term is to be added to the logarithmic formulation (3.8)

$$\delta\, 2\, test\, \left(\frac{\partial ul}{\partial x}\right)*(-\exp(ul)\,(\exp(ul)-1)(\exp(ul)-0.5)\ -2\frac{\partial ul}{\partial x}-ul\frac{\partial ul}{\partial t}) \tag{3.9}$$

Here, δ is a tuning parameter having small value. As seen from Figure 3.4, the stabilization used leads to the positive and smooth solution profile, which is just slightly diffusive at the front and tail of the pulse where strong gradients exist.
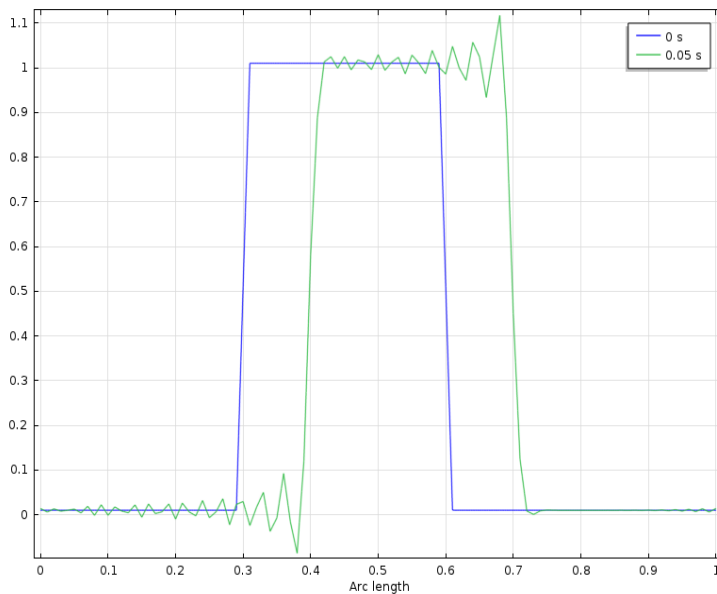

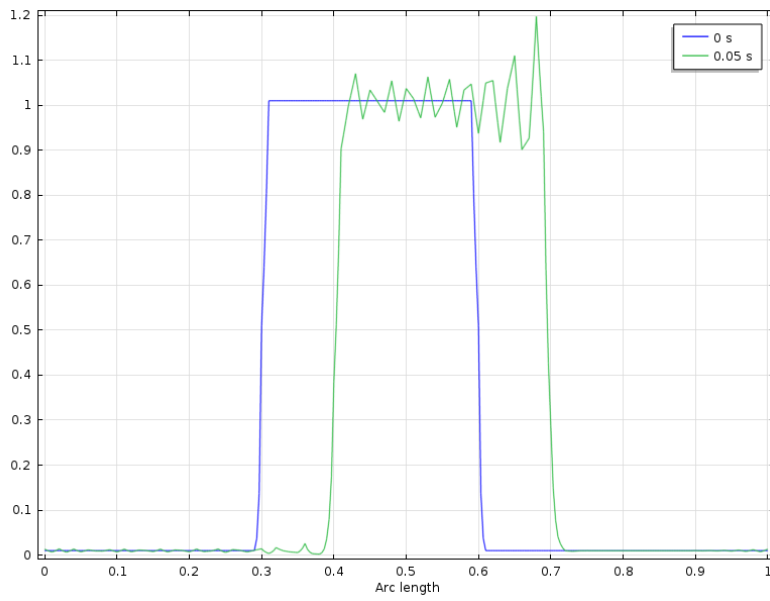Figure 3.2. Solution of the original problem (3.7)

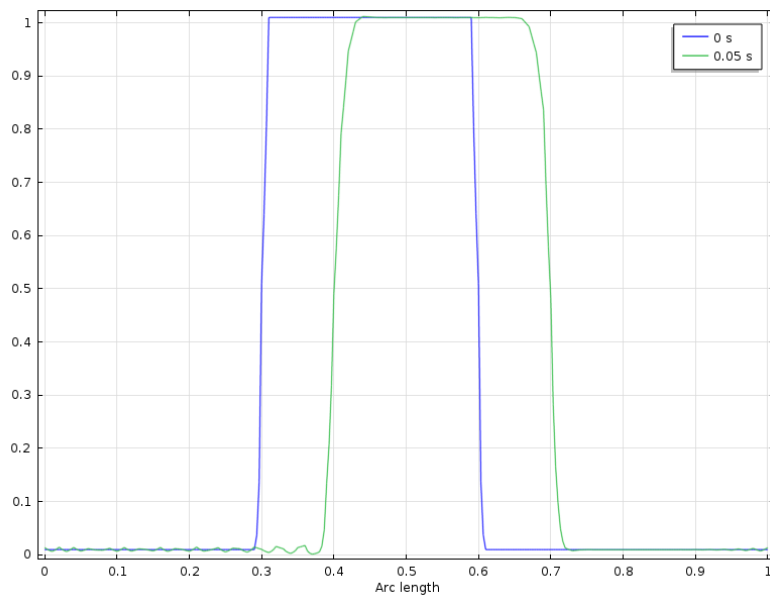Figure 3.3. Solution of the logarithmic problem (3.8)

Figure 3.4: Solution of the stabilized logarithmic problem (3.8) – (3.9).

3.4 Adaptive Mesh Refinement

The considered drift-diffusion problem consists of three transport equations with highly non-linear sources and coefficients. Solution of them is stabilized by utilizing consistent SUPG method. These equations are coupled with Poisson equation and three Helmholtz equations. Taking into account that resolving streamer head properly required mesh resolution (5-10) μm, FE discretization of all these equations yields a huge number of unknowns resulting in extremely long computational time. To reduce it, a smart meshing technique can be utilized. Firstly, one may notice that high resolution is required locally (streamer head and channel) while for the main part of the discharge volume a coarse mesh can be used. In such cases, a technique called adaptive mesh refinement (AMR) is usually employed [42]. When using AMR, the mesh is refined only in the areas where the gradient of a certain quantity of interest is high. To realize this technique, a coarse mesh is generated first throughout the domain such that a solution is achieved through various stabilization techniques. The local L2-norm error in gradients of the primary variable of all the elements is then calculated using the residuals [43]. The error indicator can be chosen as L2-norm of gradient of primary variable 'V'. The solution works the same way for L2-norm of electron density 'ne' gradient.

$$High\ Gradient\ (error)\ V = \sqrt{\left[\left(\frac{\partial V}{\partial y}\right)^2 + \left(\frac{\partial V}{\partial y}\right)^2 + \left(\frac{\partial V}{\partial z}\right)^2\right]} \qquad (3.10)$$

$$High\ Gradient\ (error)\ ne = \sqrt{\left[\left(\frac{\partial ne}{\partial y}\right)^2 + \left(\frac{\partial ne}{\partial y}\right)^2 + \left(\frac{\partial ne}{\partial z}\right)^2\right]} \qquad (3.11)$$

As a sharp gradient of the field appears at the tip of streamer head (due to space charges) and low strength everywhere else in the domain, the AMR routine is active only at the tip. The mesh is refined in the elements with the higher L2-norm (3.11). The results from the previous mesh are mapped onto new mesh and the new mesh is used to calculate the solution for the next time step. The error norm check is repeated until the defined number of refinements is reached for each time step. Since the primary quantity in the drift-diffusion calculations here is the electron number density, the error norm is defined for the magnitude of the its gradient. Thus the AMR routine refines the elements where the gradient of the electron density is high that is observed along the boundary of propagating streamer in the present study. This allows introducing a coarse mesh in almost entire domain and provide very fine mesh wherever it is needed thus reducing significantly the size of the problem and simulation time. Sometimes error norm can be defined for other quantities, e.g., the gradient of the potential that yields mesh refinement if regions where E field changes very fast that may happen e.g. on metallic surfaces (electrodes).

4 Study cases of discharges in atmospheric air

4.1 Simulations of nanosecond discharge

To validate the model and its implementation presented in the previous chapters, simulations of gas discharge have been conducted for the conditions corresponding to the recently reported experimental study [11]. The experiments were conducted in air at atmospheric pressure using needle-plane electrode system. The needle tip had a radius of 0.1 mm and 20 degrees slope that provided very high electric field strength at the tip for the inter-electrode distance of 15 mm and low field magnitudes (below the critical value) in the rest of the gap. Rectangular voltage pulses with the amplitude of 32 kV were applied. The rise time for the pulse was 150 ps and the fall time was 3 ns providing the voltage magnitude exceeding 29 kV during 10 ns. In the experiments, the pulses were repeated with the frequency of 5 kHz while in the calculations, the first pulse only was simulated to avoid effects of any preceding volumetric charges.

In [11], discharge development was recorded using a CCD camera with wavelength filter in the range 190-850 nm. The camera was synchronized with the pulse generator with the tolerance of 200 ps. An image was taken at each nanosecond interval so that the progression of the discharge could be traced in nanosecond time scale, which is needed to resolve its propagation. These images were used for verification of the developed simulation approach.

The simulation model for this case utilizes 2d axisymmetric representation of the experimental domain as shown in Figure 5.1. The drift-diffusion equations are written in logarithmic form transformed to cylindrical coordinate systems as described in the previous section. In this way, a constrain on scalar density is imposed to keep it always positive without introducing extra source terms which are implemented as described in chapter 3. The SUPG with crosswind diffusion for consistent stabilization is applied by introducing weak form contribution for the logarithmic formulation of transport equations as stated in previous chapter.

Since the solution of the seven-coupled equations (2.7-2.10) is time consuming, the domain for solving the drift-diffusion PDEs was chosen to be smaller than that for calculating the E-field based on an assumption that the influence of space charges vanishes quickly with the distance from the axis.

The boundary conditions for the different PDE's are as indicated in the figure:

- Dirichlet boundary conditions are provided for Poisson's equation (rectangular potential pulse with the rise time of 150 ps, duration of 10 ns and magnitude of 32 kV is applied to the needle and plane is grounded). The external boundaries are set to zero normal flux boundary condition.
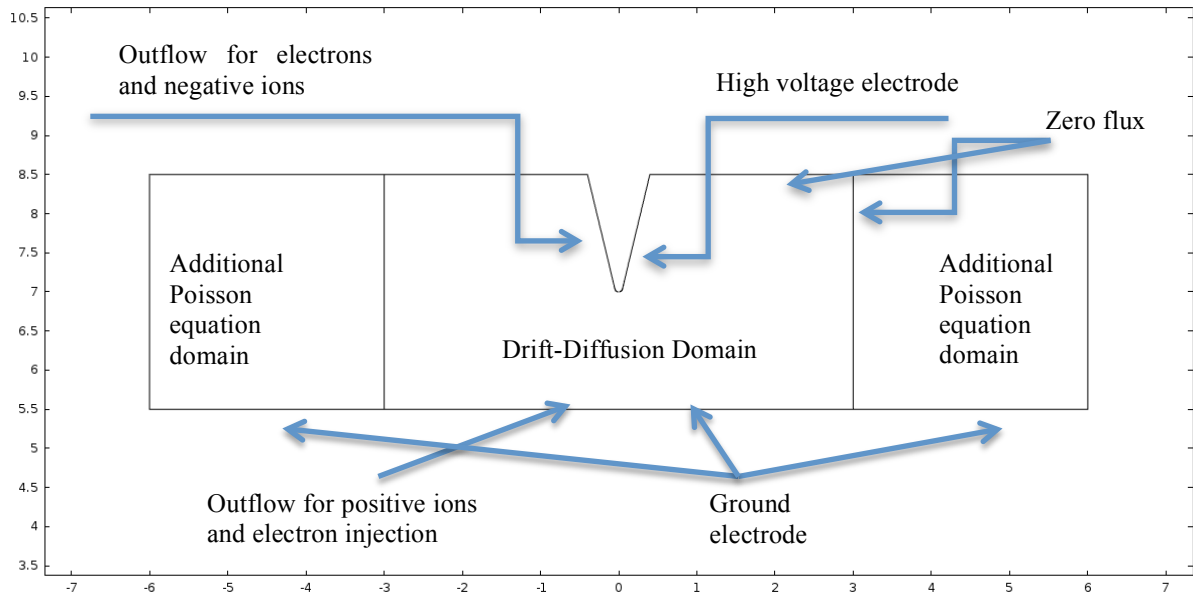
Figure 4.1: Details of the simulation model

- The drift diffusion equations are provided with outflow or zero flux boundary conditions on the electrode's boundaries dependent on the drift direction. Zero flux boundary conditions are applied on external boundary and zero radial flux on the symmetry axis. Electron emission from the cathode (bottom line in the figure) is specified as an injected flux of electrons proportional to the flux of ions scaled with Townsend's second coefficient.

Photoionization is implemented utilizing three-term Helmholtz approximation of the integral model. Helmholtz equations are provided with zero boundary conditions according to [33]. All the equations are symmetric about the central axis, which is represented as Neumann boundary for scalar dependent variables.

A triangular mesh with variable element size is introduced such that the resolution is higher at the needle than in the rest of the domain. Adaptive mesh refinement based on L2-norm of the gradient of the electron density is used to refine the mesh on discharge edge at each time step as demonstrated in Figure 4.2. This helps also in resolving sharp gradients of the density experienced at streamer head if this form of discharge appears.

The solution process involved two groups of equations, which are iteratively solved one after another to reach convergence. Poisson's equation together with the transport equations formed the first segregated group while the second one was composed by Helmholtz equations. An implicit time stepping scheme of first order [44]. Due to the strong non-linearities involved, Newton-Raphson solver with damping was used such that the Jacobian is updated on every iteration. The matrix solution is achieved through the direct solver, which allows for parallel computations.
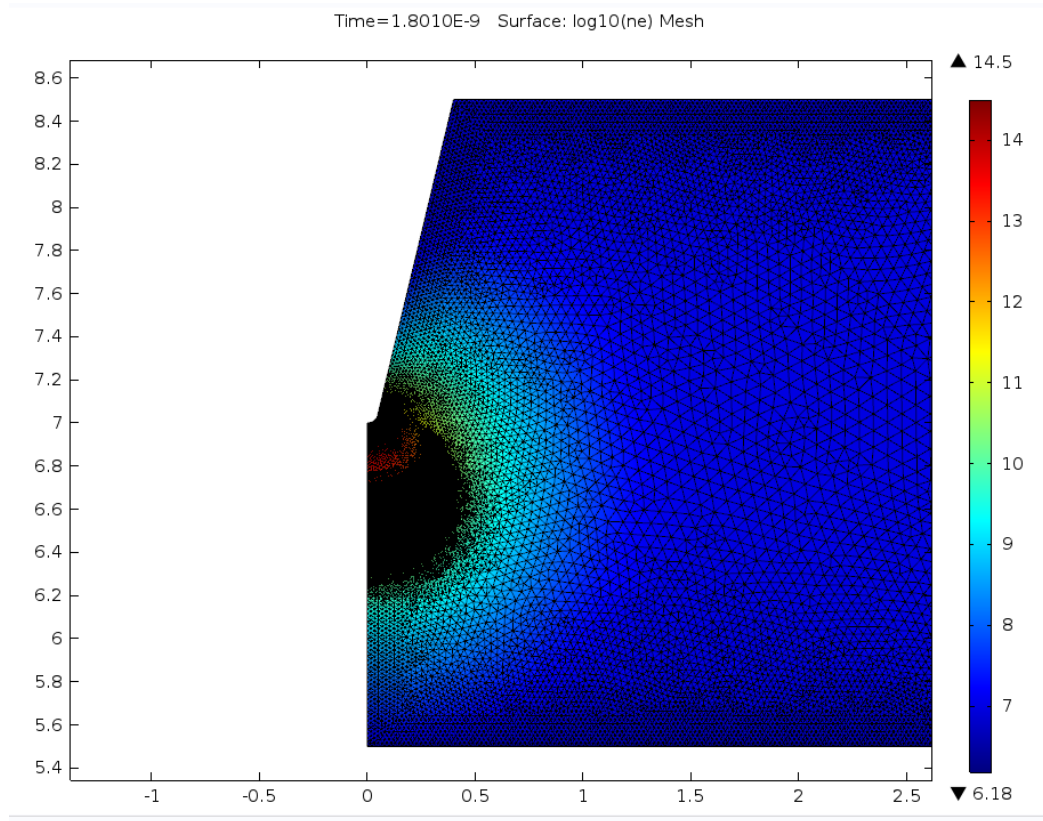
Figure 4.2: AMR on the boundary of propagating discharge overlaid with log of electron number density (cm^{-3})

4.2   Comparison of simulated and experimental results

The experimentally obtained images of the discharge [11] shown in Figure 4.3 demonstrate that as soon as high voltage is applied, a charge cloud of spherical shape is formed near the needle electrode instantaneously. It can be seen that at 1 ns it covers about 1/3 of the gap. For the next two nanoseconds the electron cloud stabilizes and there is a change in the intensity of the photon flux. Finally the cloud starts to elongate towards the cathode and bridges the gap in approximately six nanoseconds.

As it was mentioned above, the radiation intensity in air is defined as

$$I(\mathbf{r}) = \frac{p_q \xi R_{ion}}{p_{O_2} + p_q} \tag{4.1}$$

where p_q represents the quenching pressure equal to 60 Torr and ξ is the efficiency of production of photons. It can be seen that the radiation intensity is directly proportional to the ionization rate [34]. Therefore, the qualitative comparison between the experimental UV imaging and ionization rate can be correlated. In the simulations, the ionization rate is seen to have a spherical shape at first nanosecond. Similarly to changes in the recorded radiation pattern, the stabilization of electron cloud for next few nanoseconds can be seen. The elongation of this spherical cloud about the vertical axis is also observed and there is good match between experimentally measured and modeled propagating speeds. The time needed to bridge the gap between the electrodes is roughly the same in both cases (5ns).
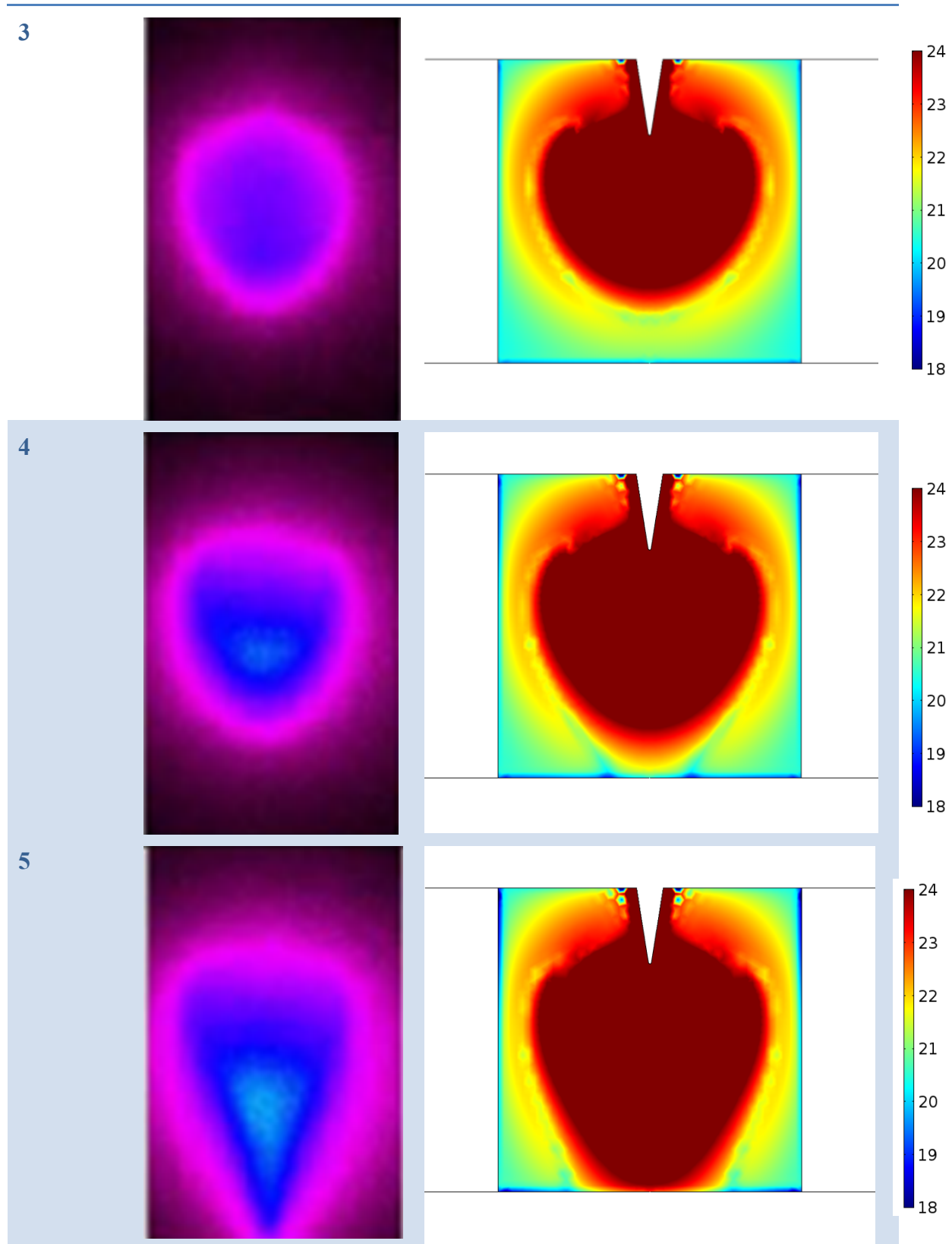
Time (ns)	Experiment	Simulation
0		
1		
2		
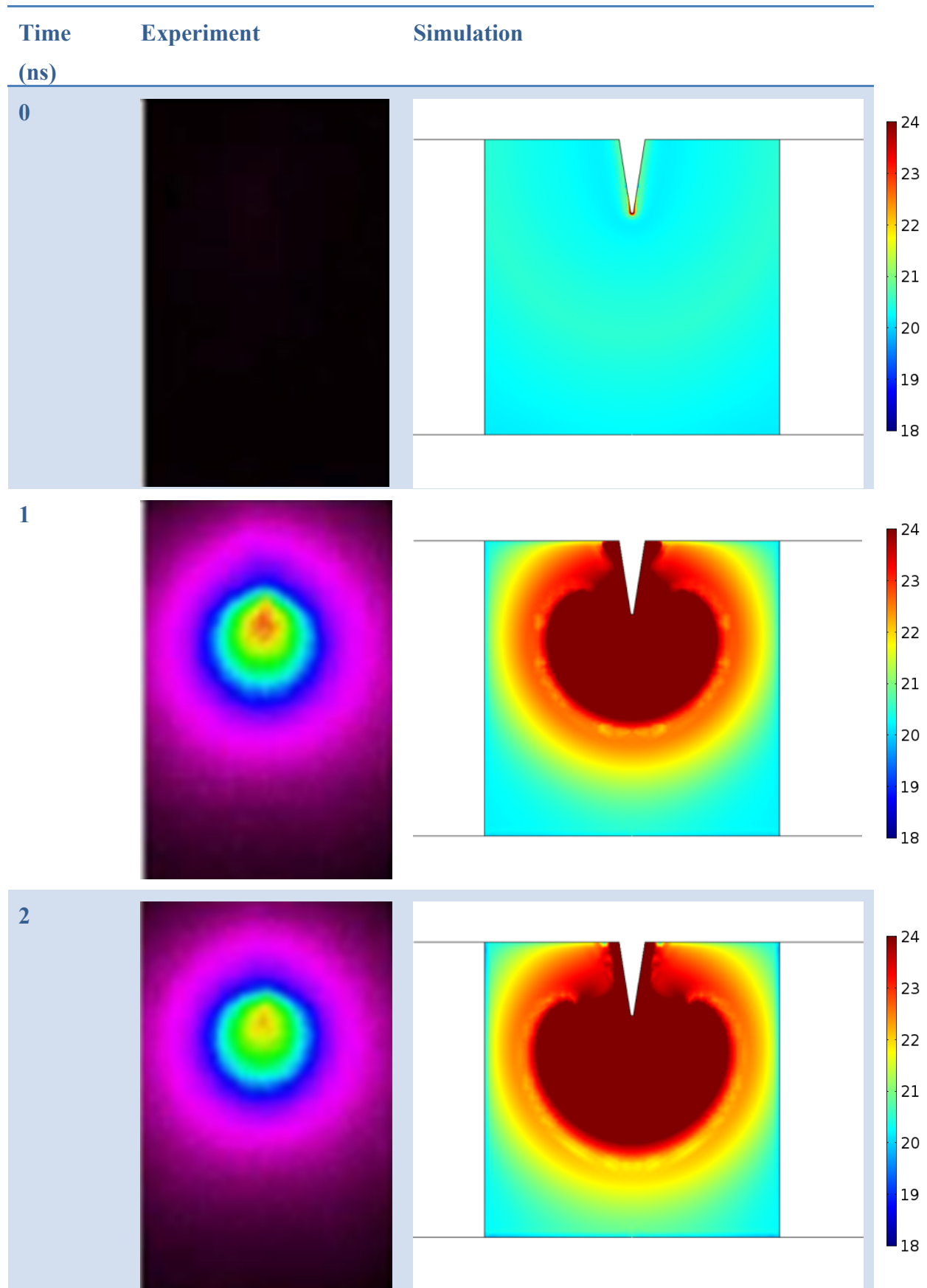
Figure 4.3: Correlation between measured radiation patterns (left column) and computed variations of radiation intensity (in legend cm^{-3}s^{-1}) distribution (right column).

The distribution of the electric field along the discharge axis is plotted in Figure 4.4. As seen, the background electric field right after voltage application is extremely high near the needle electrode. This is the electrostatic electric field with negligible effect of space charges. About 0.1 nanoseconds later, the electrons are generated in large numbers (about 10^{19} - 10^{20} m^{-3}) such that a spherical shape is formed as shown in Figure 4.3. Because of the space charge created at the needle tip, the E-field is screened out and drops to a low value of about 100 kV/cm. This value matches well-known literature data, see e.g. [2, 3, 12, 25, 39, 45-48]. The photoionization takes place in front of the local field peak and start providing photoelectrons. This causes electronic cloud to move forward towards the cathode. The motion of the maximum of the electric field in Figure 4.4 is associated with the propagation of the front of the space charge cloud. Similarly figure 4.5 shows the propagation of electron density for the same electron cloud along the axis.
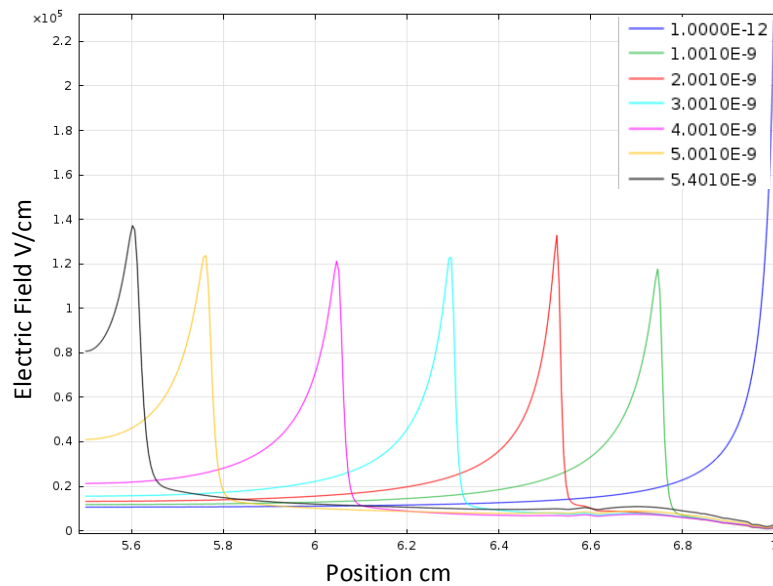

Figure 4.4: Electric field along the axis over time (shown in the legend in seconds). The needle tip is located on the right hand side.
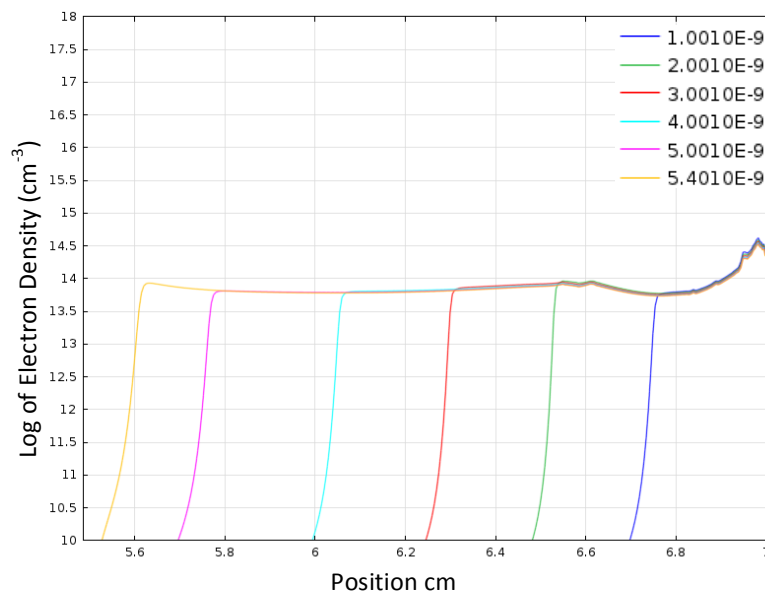

Figure 4.5: Electron number density (log) along the discharge axis over time (shown in the legend in seconds).

4.3 Streamers in air - comparison with earlier performed simulations

Implementation of streamer propagation model in Comsol Multiphysics similar to the one described in chapter 3 has been attempted earlier [12]. In that study, several methods were utilized to overcome the numerical challenges discussed above e.g. introducing additional auxiliary source terms, manual mesh refinement, etc. This has allowed for simulating streamer propagation in air in short (5 mm) and long (30 mm) gaps in a needle-plane system that yielded reasonable agreement with experimental results. Note that the length of the streamer is used in electrostatic sense meaning the strength of its interaction with electrodes (it is stronger for a short streamer). In this study, several issues have been noticed like long computational times, needs for increasing accuracy of the simulations, necessity for adaptive mesh refinement, etc. All these problems are dealt with in the present work and, therefore, it is of interest to repeat the simulations presented in [12] with the new method and to compare the results with those obtained with the reference model.

Streamer propagation in atmospheric pressure air between needle and plane electrodes separated on a distance of 5 mm is considered in 2d axisymmetric model as shown in Figure 5.6. Similarly to [12], a step of voltage of 15 kV with rise time of 0.1 ns was applied between the electrodes. The boundary conditions used are indicated in the figure. Note that in the new model the domain for solving Poisson's equation is extended. The physical source terms in the drift-diffusion PDEs are the same as in the reference model while those, which were artificially introduced for stabilization purposes, are removed in the present model. The contribution from diffusion of ions is also neglected due to the short duration of the discharge event. Note that the new model utilizes the logarithmic formulation of the transport equations and SUPG and crosswind consistent stabilizations are added. In addition, three-term Helmholtz approximation is introduced instead of two-terms used in [12] that enhances the photoionization model as the fit is better with the integration formulation [34].
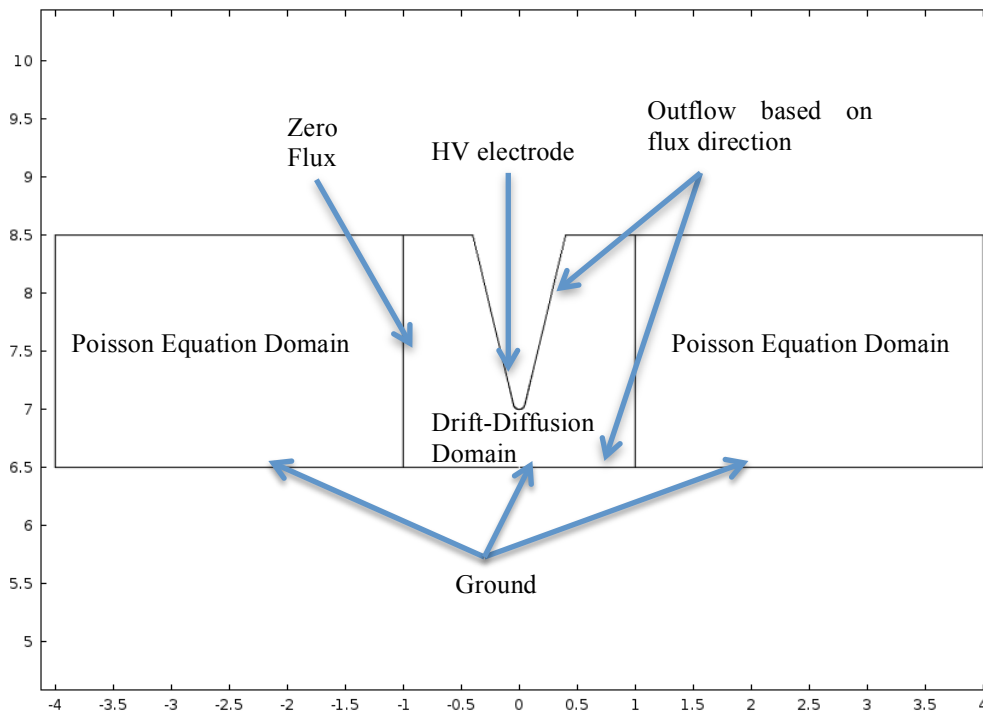

Figure 4.6: Geometry and boundary conditions used in the model.

Calculated time variations of the electron density patterns are shown in Figures 4.7. The electron density is plotted for 0.5 ns, 1.5 ns and 2 ns similarly to the reference model. The shape of the streamer channel and its growth rate are comparable. The time needed to bridge the gap in the reference model is 2.15 ns whereas in the present model it is 2.3 ns. Note that Gaussian charge spot used as the initial condition for streamer inception in the earlier model is not used in the new simulations. Instead, the process started from uniformly distributed charges carriers appeared due to background ionization. After voltage application, the local electric field causes the electrons to quickly get absorbed at the anode leaving aside positive charges causing initiation of streamer formation. This process needs about 0.2 ns to develop and produces a spike in current measured during experiments [24]. On this stage, the electron density grows as a sphere surrounding the tip of the needle electrode (anode). Later on, the electronic cloud expands towards the plane (cathode) due to generation of electrons in the streamer head and after few nanoseconds the streamer bridges the entire inter-electrode space. The calculated diameter of the plasma channel during streamer propagation is comparable in both cases.
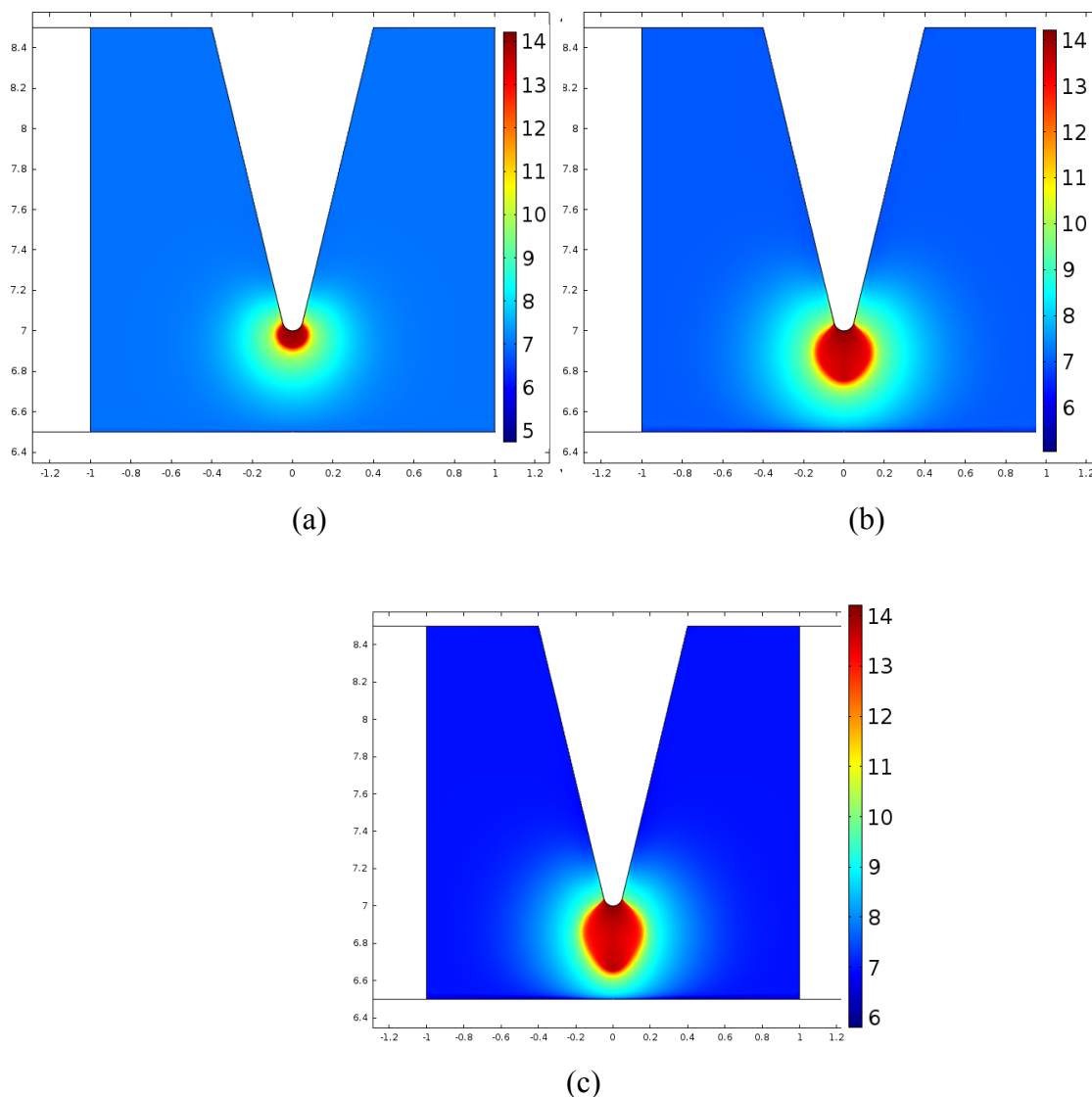
.

(a)   (b)

(c)

Figure 4.7: Log of electron number density (cm^{-3}) at 0.5 ns (a), 1.5 ns (b) and 2 ns (c)

The electron density profiles along the axis of the discharge are show in Figures 4.8 and 4.9. As seen, the developed model yields magnitudes of the densities, which are in agreement with those obtained with the reference model. Also, the steep gradients of concentration at the front are well described. Some disagreement in the results can be observed behind the propagating from in the bulk of the streamer. This, however, can be a numerical drawback of the old model where the radial expansion of the channel was not properly controlled.

.
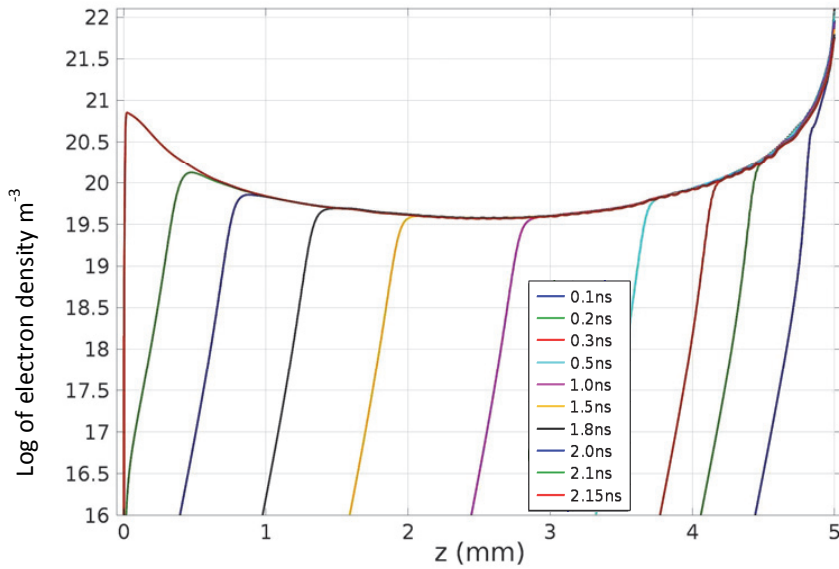
Figure 4.8: Electron density distribution (m^{-3}) along the axis calculated by the reference model [12]
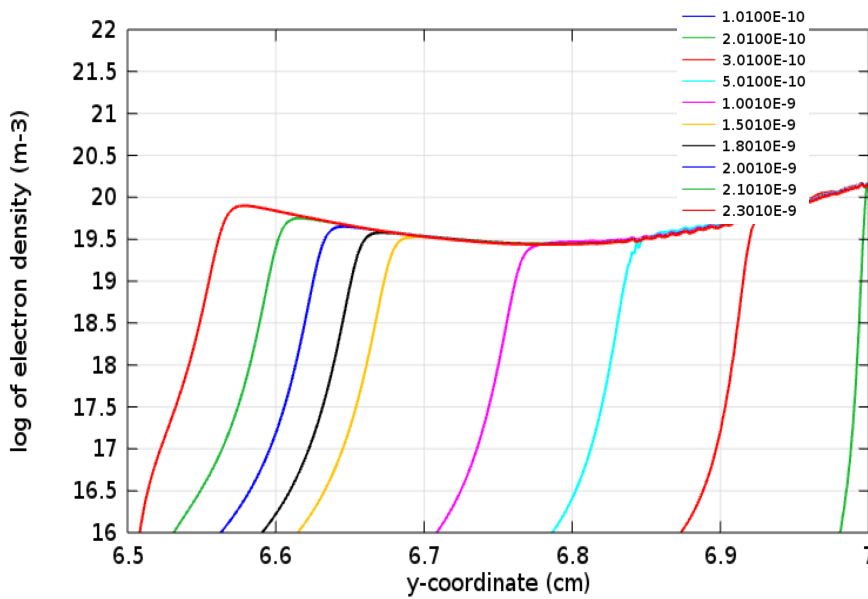

Figure 4.9 : Electron density distribution along the axis obtained with the new model

The calculated electric field patterns, Figure 4.10, demonstrate propagation of a high field region at the streamer tip, which is often referred to as an ionization wave in the literature. The distributions of the field strength along the axis of the streamer channel obtained with different models (shown in Figures 4.11 and 4.12) are comparable. However, the parameters such as maximum field strength and velocity have small differences. Thus one may notice that the maximum field strength calculated in the present study is higher than that obtained in the previous model. This may be related to different treatment of the photoionization term in the two models that is in general more accurate in the present work [34] providing a very localized source of charged species at the propagating streamer front as shown in Figure 4.10 The small region of strong photoionization source next to streamer head is known to cause smearing of electric field front [49].
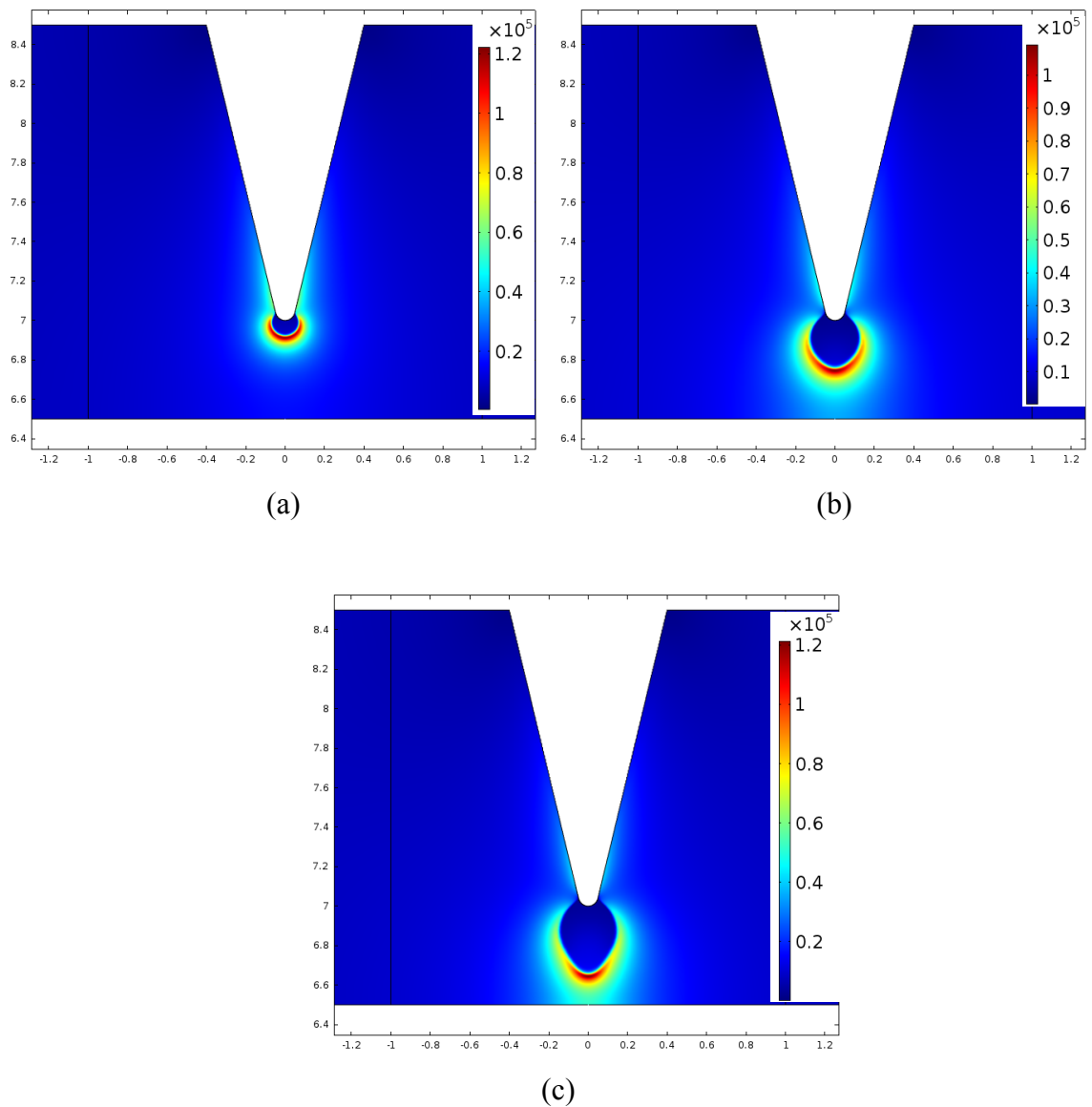

(a)

(b)

(c)

Figure 4.10: Evolution of the electric field (V/cm) at 0.5 ns (a), 1.5 ns (b) and 2 ns (c).
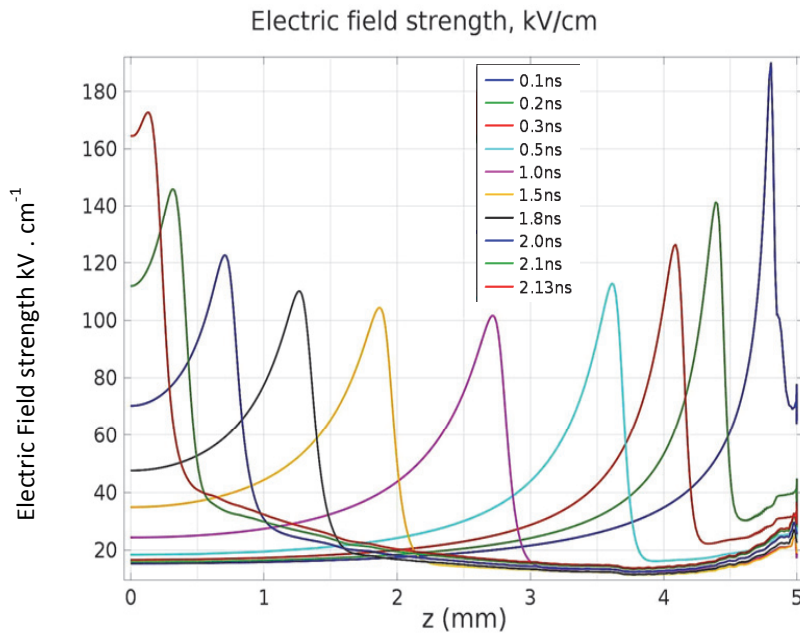
Figure 4.11. Electric field distribution along the streamer axis obtained from the reference model
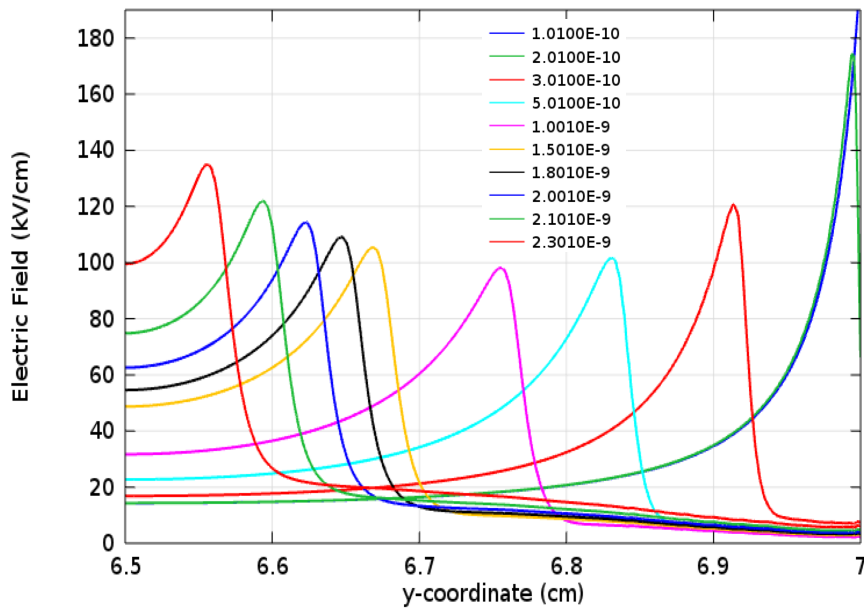

Figure 4.12. Electric field distribution along the streamer axis calculated with the new model

For the case of the long streamer, the main features related to the correlations between the results from the two models are basically the same as for the case of short discharge. The simulations compared below were performed for 30 mm air gap between needle and plane electrodes energized by applying a ramped voltage of 40 kV with a rise time of 0.1 ns. All the other model parameters are similar to the simulations presented above (for 5 mm gap) for old and new calculations. Another point to mention is that the in the old simulations, so-called overlapping mesh technique was utilized where a frame with a very fine mesh (resolution ~5 micrometer) was placed around the streamer head while a relatively rough mesh was used in
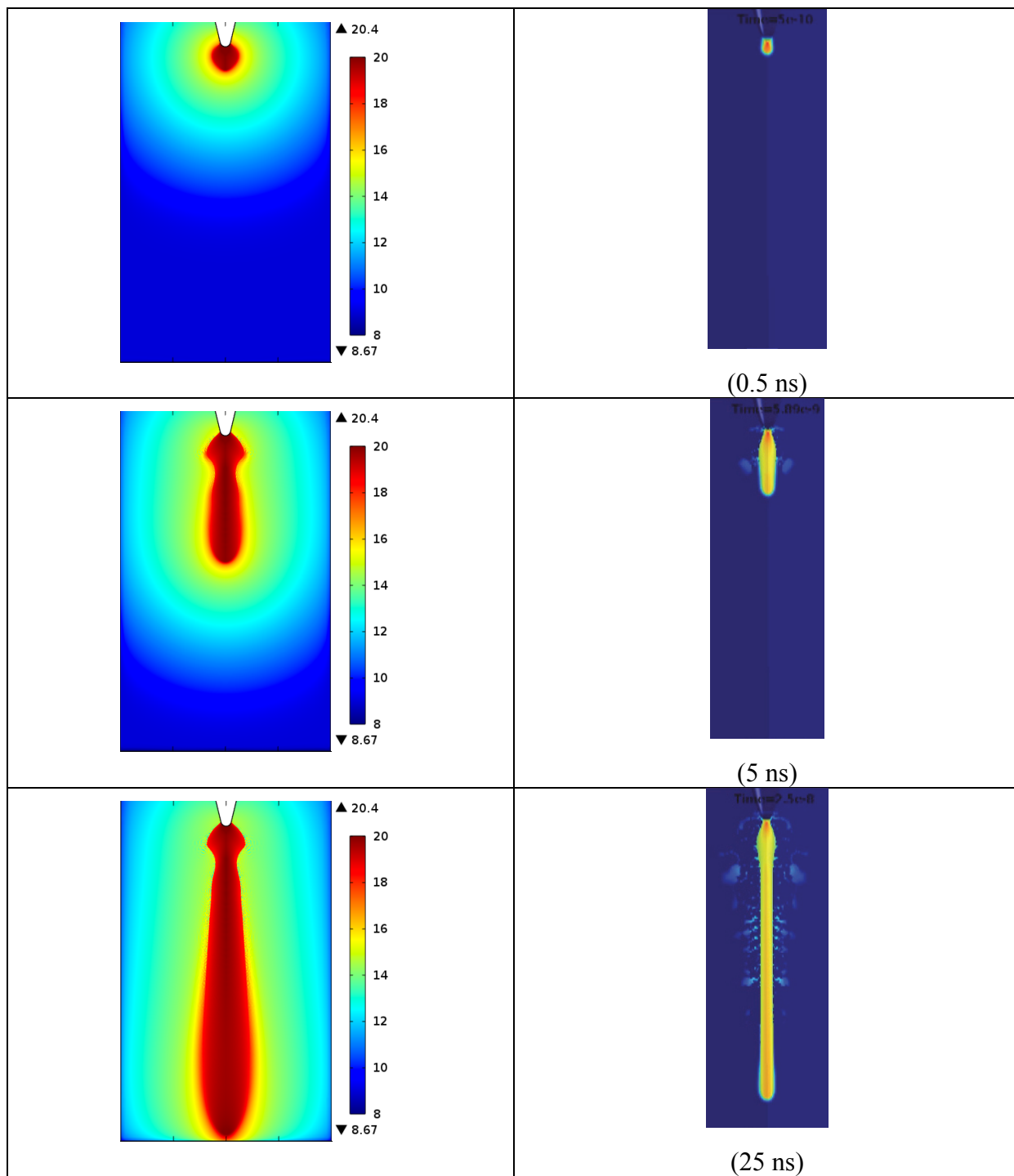
Figure 4.13: Log of electron density (m^{-3}) obtained from the new model at 1 ns , 5 ns and 10 ns on the left column compared with reference data.

the rest of the domain. When the streamer head was about to leave the region of the fine mesh during propagation, the simulations were interrupted, the frame with fine mesh was brought in front of the head, the solution was mapped into the new mesh and the calculations were continued. This approach, despite of been pure artificial and thus inconsistent, allowed for resolving steep gradients at the discharge plasma front. Since the charge species fluxes were

uncompensated each time when re-meshing the domain and mapping the solutions on an updated computational mesh (see below for a description of the associated affects), this technique was not used in the simulations with the new model. Instead, adaptive mesh refinement routine was utilized as explained in chapter 2. The error estimate is evaluated for each time step so that the streamer head can be properly resolved.

The calculated electron density patterns are shown in Figures (4.13) for the instants 1 ns, 5 ns and 10 ns. The only similarity with the short streamer described above is the development of the spherical electron cloud on the anode tip. Later on, the channel elongates along the gap with very little radial growth. The streamer needs about 10 ns to cross the gap, which is consistent with streamer propagation velocities reported in the literature [1, 11, 13, 50]

It is seen that the orders of the magnitudes of the electron densities obtained with the reference model and new model are comparable. What differs is the shape of streamer channel. In the reference simulation [12], formation of a cylindrical channel is achieved with practically constant radial dimension during entire propagation. Note also the radial spikes of electron concentration, which are pure numerical artifacts and resulted from the re-meshing of the domain in the old model. The new model yields a discharge channel, propagation of which towards the plane electrode is associated with a radial expansion. This behavior is more realistic and such channel profile matches results of other publications [39]

The electron density along the streamer axis is plotted in Figure 4.15. The results show that the streamer channel maintains almost constant density of electrons throughout the length in the central core region and there is a sudden falloff to lower density at the streamer tip and radial direction. As there is no artificial charge generation and inflow boundary condition the electron density drops to low values throughout the domain, other than the streamer channel (10^{12} m^{-3}). This density start to rise slightly as streamer approaches the cathode.

The peak magnitude of electron density $\sim 10^{20}$ m^{-3} though remains comparable to that of short streamer. Also the initial propagation speed of streamer is slow for first nanosecond as seen in Figure 5.17, but thereafter the streamer maintains a constant speed of about 2.5 mm/ns up till the bridging of gap at 11 nanoseconds.

Similarly to the case with short streamer, the maximum electric field strength magnitudes obtained from the new model are higher than in the old simulations (Figure 4.16). This can be related to different treatment of photoionization term in the drift-diffusion equations providing that the lower rate of production of photoelectrons yields higher electric field, but at the same time, provides seed electrons the number of which is just enough to maintain streamer propagation. It is notable that the average streamer velocity obtained with the new model is ~ 3 mm/ns whereas it was ~ 1 mm/ns in the old model. As stated above, this difference can be due to higher electric field in the new model and different photoionization models used.

The electric field magnitude is plotted along the axis at different time instants in Figure 4.18. The electric field is very high in a narrow region at the streamer tip. The peak magnitude is higher than 10^5 V/cm for the duration of streamer propagation and rises to $1.5 \cdot 10^5$ V/cm when the streamer reaches the cathode. The peak magnitude is comparable to the literature data available for streamers in air [30, 51]
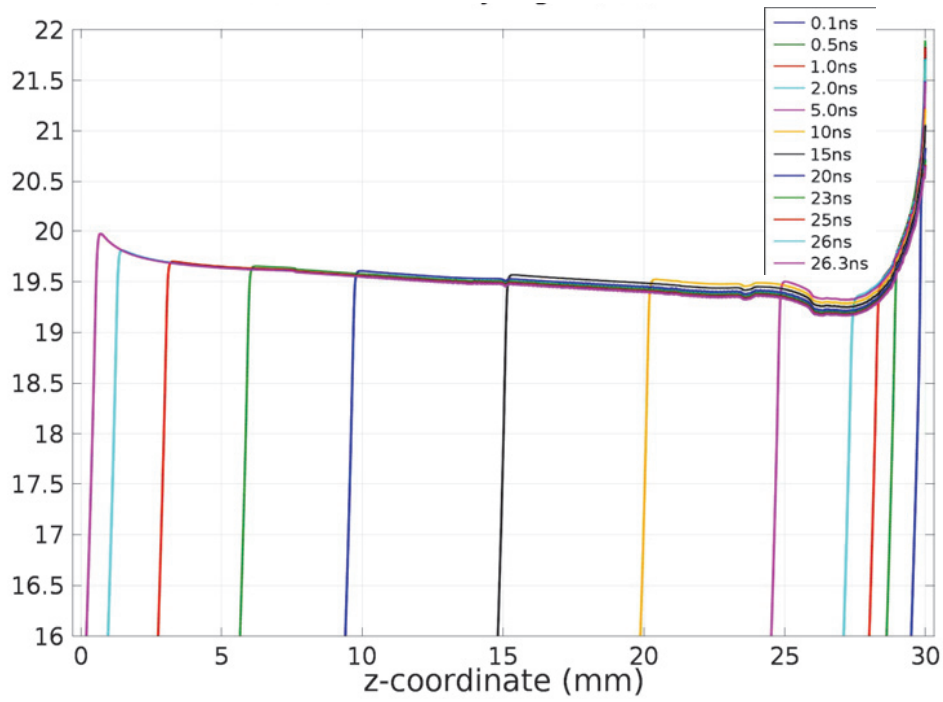
Figure 4.14: Electron density along the axis at different instants (seconds) in the reference model
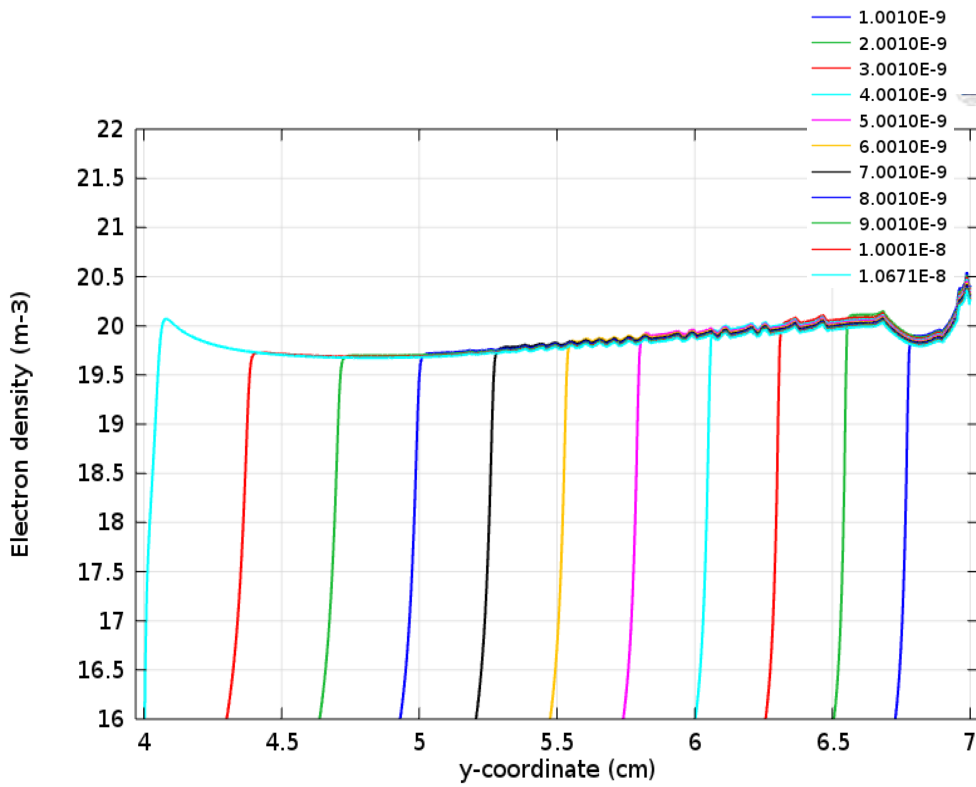

Figure 4.15: Electron density along the axis at different instants (seconds)
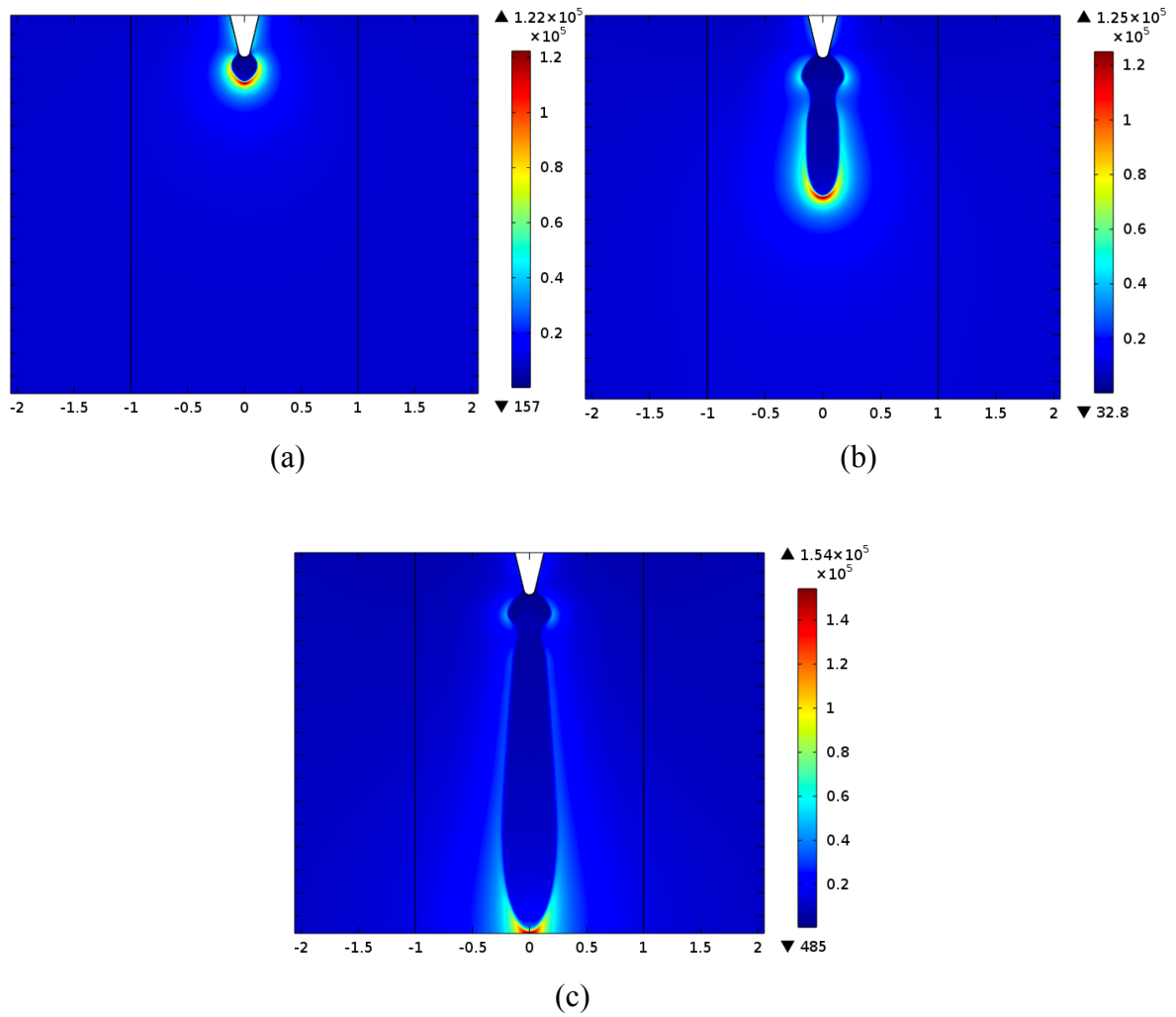
(a)

(b)

(c)

Figure 4.16: Electric field strength patterns obtained with the new model at 1 ns (a), 5 ns (b) and 10 ns (c).
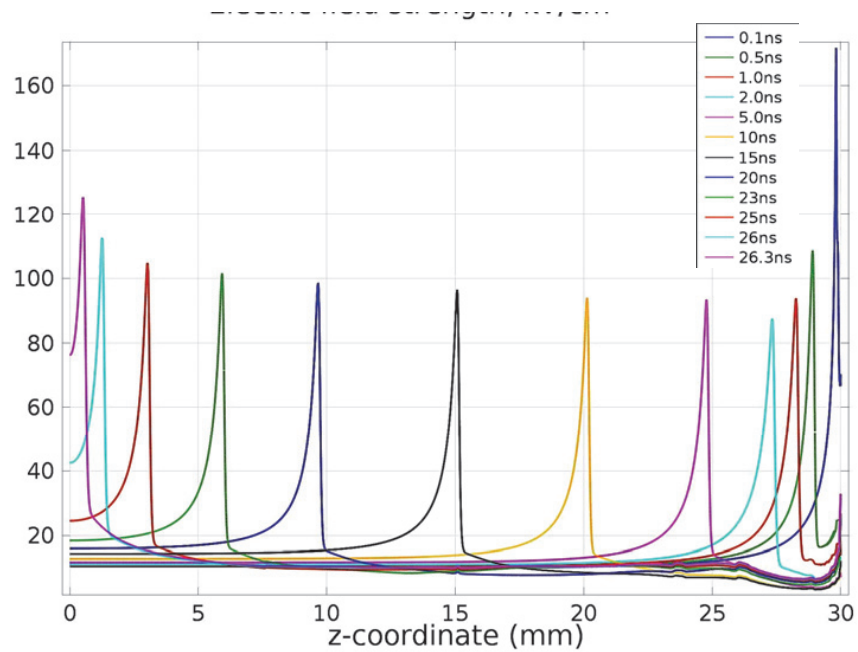

Figure 4.17: Electric field strength along the axis (kV/cm) at different instants in reference model
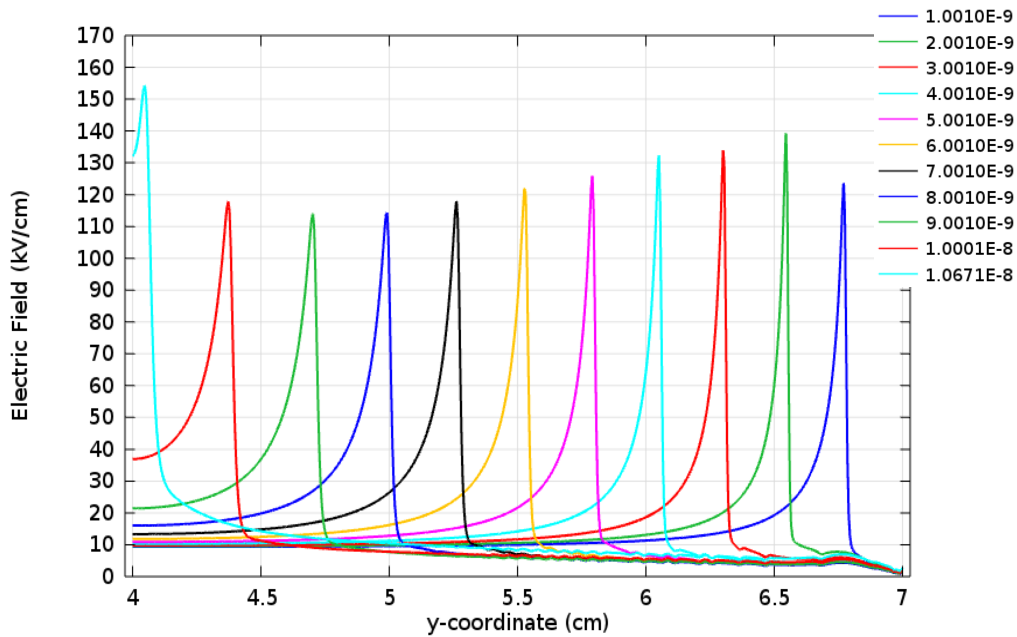
Figure 4.18: Electric field strength along the axis (kV/cm) at different instants

4.4 Non-axial streamer propagation

A case of non-axial streamer discharge propagation between two parallel round disc is considered. The disc shaped electrodes with filleted edges of 0.5 mm separated by a distance of 10 mm are immersed in dry air at atmospheric pressure as shown in Figure 5.20. Since a symmetrical geometry is modeled, the domain can be reduced by using axial symmetry. In reality, the problem is three-dimensional since the discharge channel has a finite size in the direction normal to the plane. Hence, two-dimensional approximation to the real situation is considered here.

A positive DC step voltage of 35kV is applied on the top electrode and the other electrode is grounded (Poisson equation boundary condition). The flux boundary conditions specifying outward flux is considered when the charged species are moving towards the disc-electrode whereas zero flux boundary condition is used when they are moving away from external boundary. All the other boundaries uses zero flux boundary condition for drift diffusion transport equations. The treatment for photoionization boundary conditions is based on dirichlet formulation with zero values on all boundaries [33] .Uniform initial charge densities are applied similar to the previous models. AMR as discussed before based on L2-norm of electron density gradient is used to resolve the streamer head.

The calculated electron density patterns at streamer initiation and propagation are shown in Figure 5.23. As seen, the streamer inception takes place in the region of highest electric field at the curved surface of positive energized electrode and it propagates to the grounded one. The discharge channel expands in first few nanoseconds and then starts moving along the field lines. The peak electron density during propagation is ~10^{13} cm^{-3} that is slightly lower than that for symmetrical streamers discussed above. After ~4 nanoseconds streamer channel starts deviating from the E-field line turning inwards towards the axis. Just before this, the local electric field on the ground electrode gets enhanced due to the potential induced by the approaching positive streamer head that leads to inception of a negative streamer.
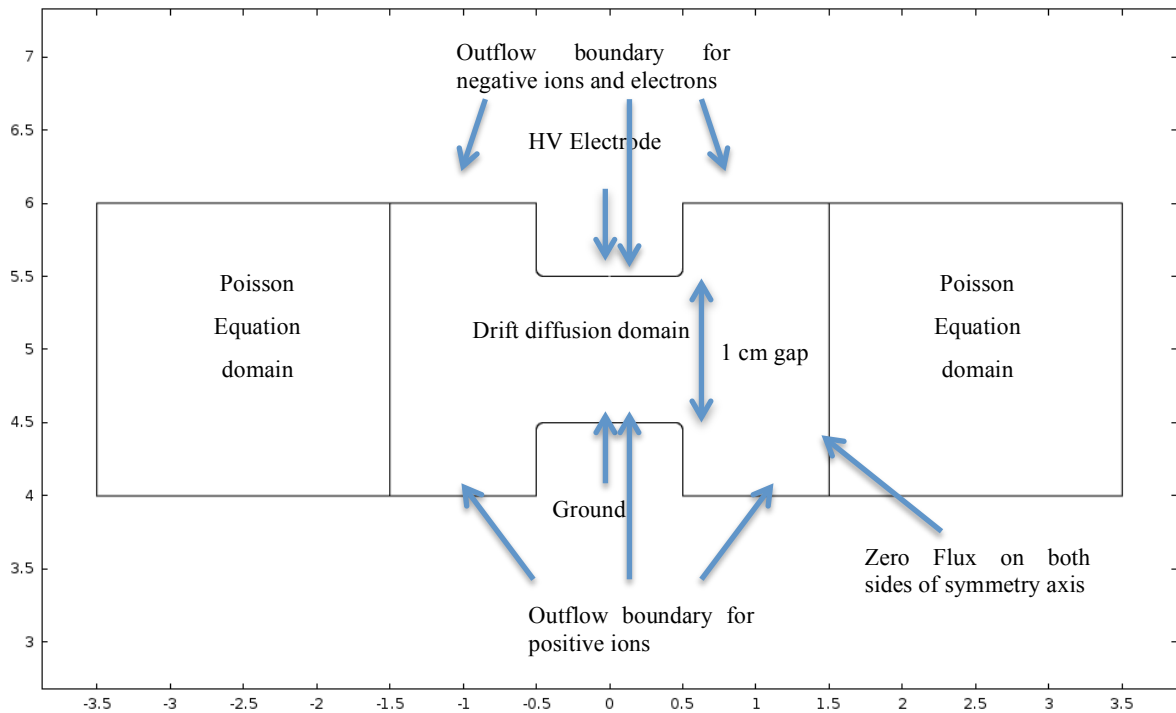
Figure 4.19: Flat disc model details

The streamers move towards each other and finally meet forming a continuous channel bridging the gap between the electrodes. At this stage, the peak of electron density reaches ~10^{15} cm^{-3}.The electric field distributions for different time moments are plotted in Figure 5.24. It can be seen that streamers heads are resolved properly and there are no numerical artifacts anywhere in the calculation domain. The peak electric field magnitude is in the range of 10^5 V/cm and it is highest in the narrow regions at streamers heads and lowest behind them within streamers channels. The field is fairly stable in magnitude during initial propagation stage up till the positive and negative streamers approach each other. After this instant, no further enhancement is observed. The averaged streamer front propagation speed is ~2 mm/ns, which matches other experimental and simulation data. It is interesting to note that the non-axial propagation leads to the change in direction of the positive streamer channel, which is not observed in axially propagating discharge. This time resolved simulation of non-axially propagating streamer enhances understanding of breakdown phenomena in practical electrodes configurations and can be used for developing empirical formulations of breakdown criteria.
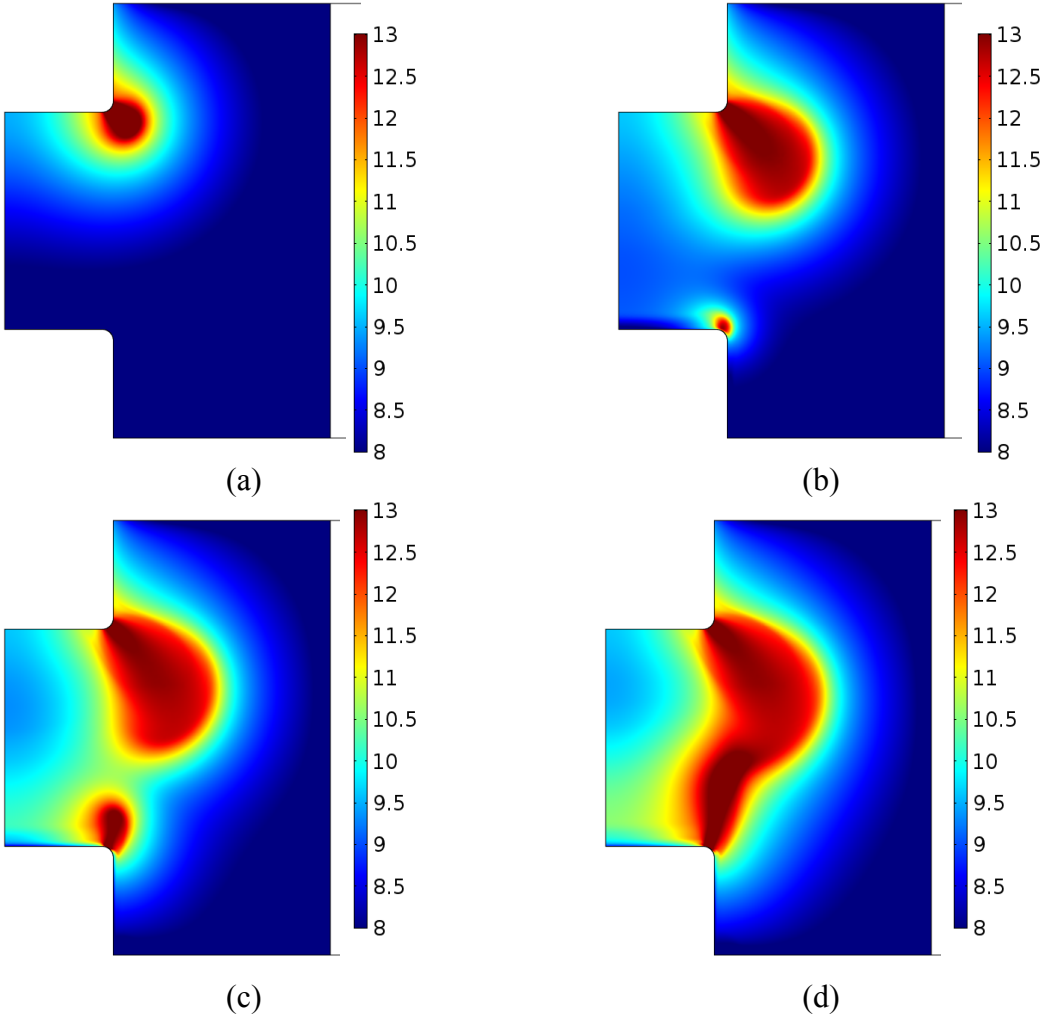
Figure 4.20: Electron density profiles at times 1 ns (a), 3.2 ns (b), 4.2 ns (c) and 4.8 ns (d). Note that the color bar scale is fixed to enhance visualization.
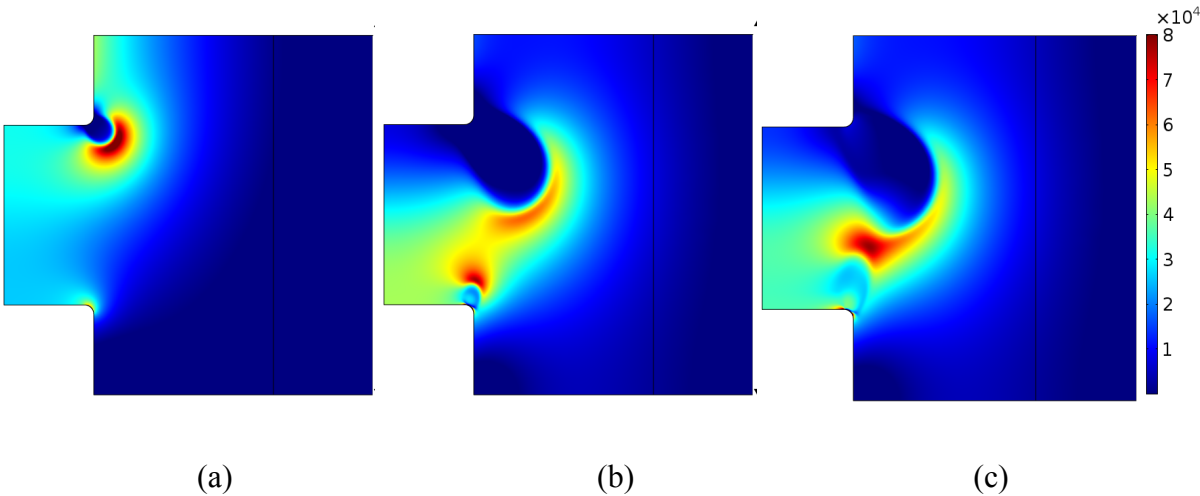

Figure 4.21. Electric field distributions at time moments 1 ns (a), 4 ns (b) and 4.8 ns (c).

5 Simulations of streamer and streamer branching in 3d domain

It is well-known that development of a streamer, especially for long distances, is associated with its branching into multiple channels. An example is shown in Figure 5.1 borrowed from [52]. Reasons for this phenomenon are not absolutely clear, but several theories have been proposed, which consider inherent instabilities at the streamer head due to probabilistic nature of gas particles, influence of inhomogeneities in gas, localized charge centers, etc. [53]. Early attempts to simulate the process were based on simple 2-d models with fixed conductivity of streamer channel [54]. Later on, streamer branching was introduced in single channel models [55]. Effects of deterministic charge distributions on streamer development were also modeled [56]. There are serious shortcomings in simulation approaches used. First of all, branching is essentially 3d phenomenon and can't be properly treated with 2d models. The 'Laplacian instability' hypothesis [55] is essentially being pushed for the 2d-axisymmetric model. It is assumed that the localized charge density at the streamer tip leads to multiple local electron avalanches and, hence, the branching. No special treatment has been done in the drift-diffusion equations for the development of these instabilities. It has been further interpreted as numerical artifacts by some peers [57]. Another probabilistic model based on the fixed conductivity of streamer channel interprets its growth in fixed step. A critical electric field is defined on the streamer tip and it grows by fixed amount in the 'probabilistic' direction based on defined 'fluctuation' [58]. This allows the streamer to 'branch' in small region by allowing it to grown in the direction, which is not the original electric field direction. This scheme though allows for branching but it is due to 'artificial' numerical treatment. The 3d branching of streamer has been attempted for liquid dielectrics based on random charge centers in the volume [56]. The branching happens when the moving streamer head sees these charge centers and splits. The stochastic models are not based on any study of local perturbations and magnitudes of distributed charges are in general unknown.
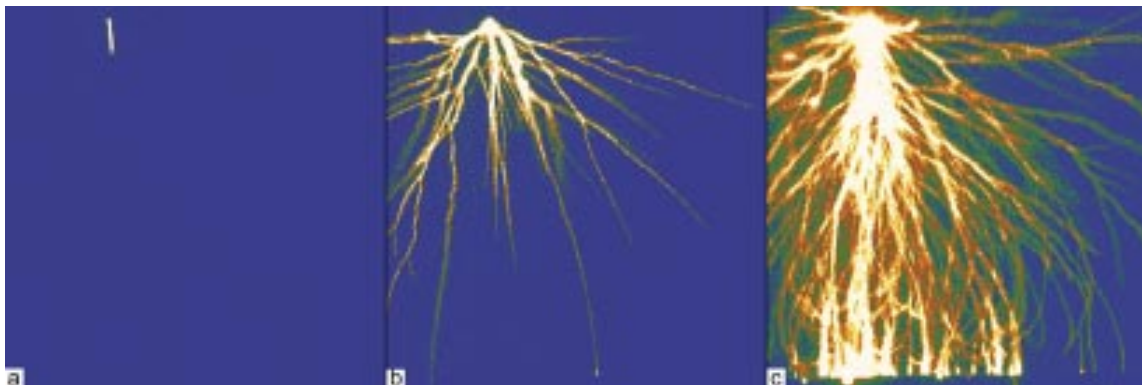

Figure 5.1: Time integrated pictures of streamers in a 25 mm, point-to-wire gap in ambient air at (a) 6 kV, (b) 12.5 kV, and (c) 25 kV.
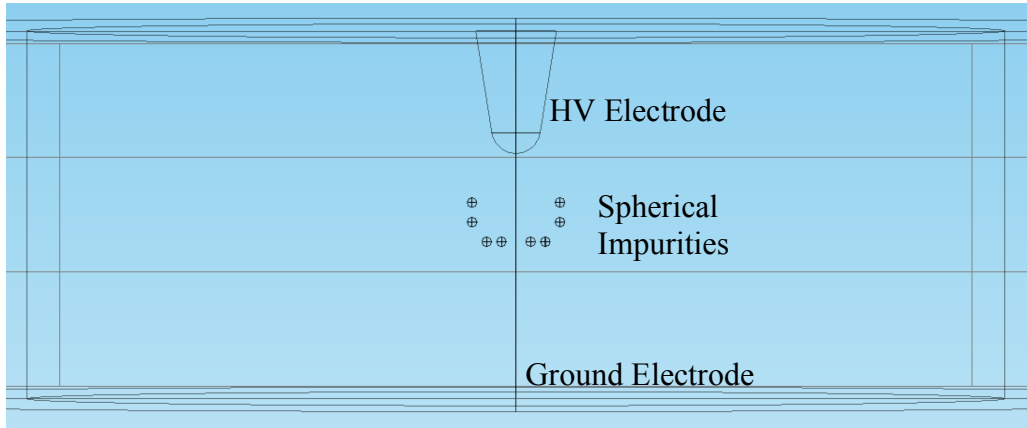
Figure 5.2: 3d simulation domain for streamer branching

To overcome these limitations, an attempt of fully 3d simulations of streamer branching was undertaken in the present study. The model of branching is an improvement of [56] where presence of local charge centers in liquid is suggested. In the present analysis, charge magnitudes are derived from inherent discharge processes without introducing any artificial approximations. The charge accumulation centers are introduced as dielectric inhomogeneities in the medium appearing due to suspended particulate (dust particles, clusters, etc.) providing local field enhancements in gas volume and thus affecting streamer propagation [56].

The simulations were performed in 3d domain formed by needle and plane electrodes immersed in air at atmospheric pressure and separated on a distance of 1 mm as shown in Figure 6.1. The needle tip radius is 0.5 mm. A ramped potential of 2kV is applied to the needle electrode and the other electrode is grounded The model implementation is similar to previously considered study cases including adaptive mesh refinement, numerical stabilization and extended domain for calculations of electric fields.

Charge accumulation centers are introduces as small spherical solid domains located at some distance away from the path of single channel streamer discharge. The surface of these spherical domain allow for charge accumulation which is modeled by discontinuity in local displacement field

$$-\text{n.}\,(\boldsymbol{D_1} - \boldsymbol{D_2}) = \rho_s \qquad\qquad (6.1)$$

where $\boldsymbol{D_{1,2}}$ are vectors of electric displacement in air and solid inclusion, respectively; $\mathbf{n}$ is the unit normal vector; ρ_s is the surface charge density. The surface charge is calculated from the normal incoming flux of volume charges

$$\frac{d\rho_s}{dt} = \Sigma_n J_n \qquad\qquad (6.2)$$

where J_n is the corresponding normal current density.

In order to have a controlled setup and to detect any numerical artifact, the simulation is first run without including the inhomogeneities. The boundary conditions are same as described before for the 2d-models, but applied on the surface. The streamer growth in the form of electron density iso-surface of 10^{12} cm^{-3} over time is shown in fig 5.3.The simulations yield a single streamer channel developing from the needle to the plane electrode as seen from Figure 5.3. The electron density is in the range of 10^{14} per cm^{-3}. The iso-surface of electric field

<div align="center">(a)   (b)   (c)</div>

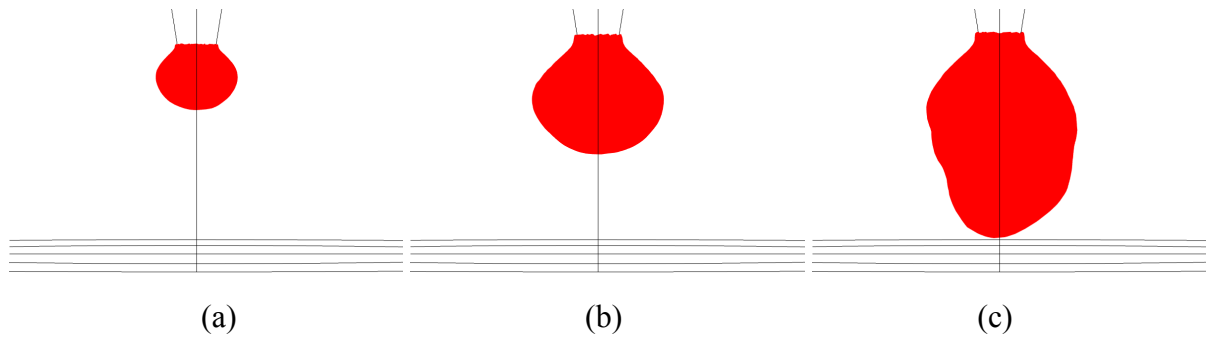Figure 5.3 : Electron density iso-surface (10^{12} cm^{-3}) plotted at (a) 1 ns (b) 3 ns (c) 6 ns

<div align="center">(a)   (b)</div>
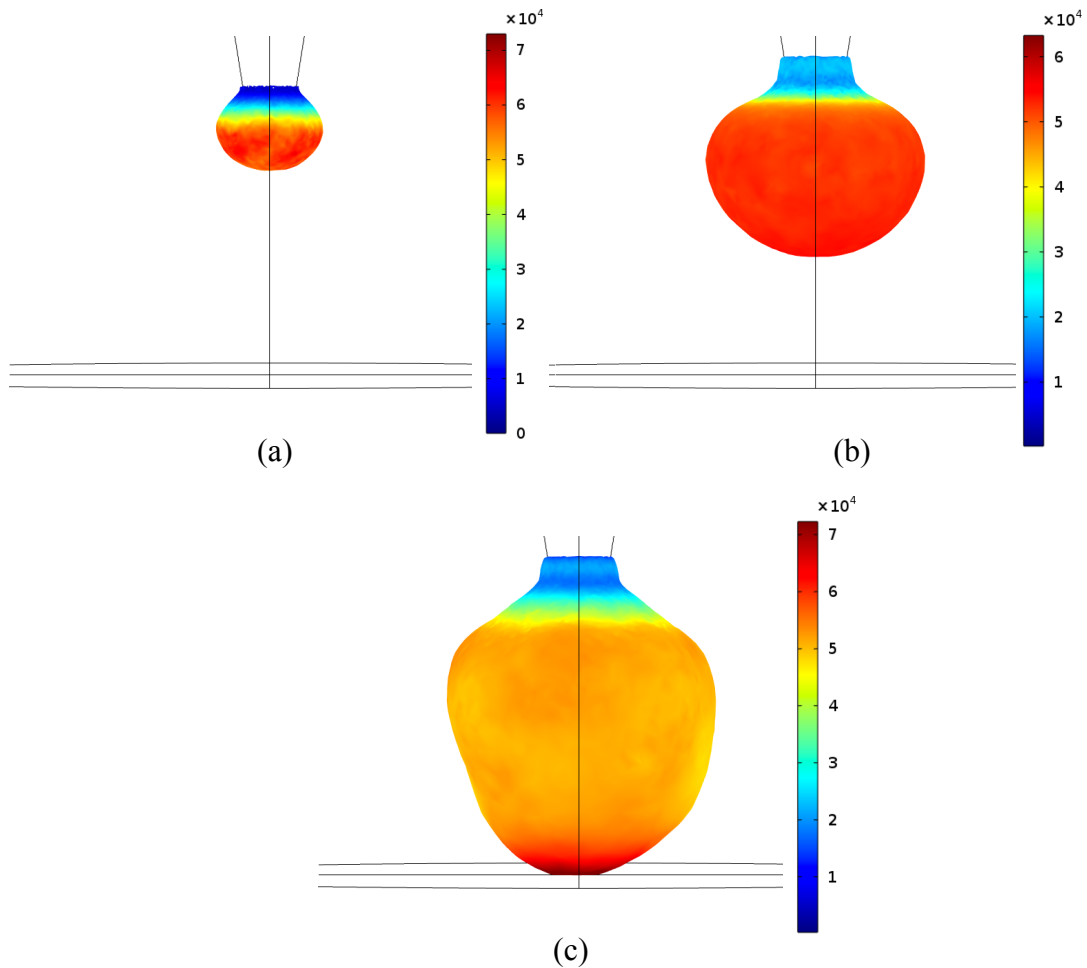

<div align="center">(c)</div>

Figure 5.4 : Electric field iso-surface plotted at (a) 1 ns (b) 3 ns (c) 6 ns

is plotted over time in Figure 5.4. The peak electric field is in the range of 10^5 V/cm, which is comparable with results in other publications.

The obtained results confirm that the dependent variables are suitably resolved in the 3d simulations so that any instability due to numerical discretization is avoided. The verification of 3d model lead to the second simulation as stated before with the inclusion of inhomogeneities and charge accumulation on these surfaces.

With the inclusion of dielectric inhomogeneities, the streamer moves away from the centrally defined base channel as seen in Figure 5.5. This is due to the fact that the electric field magnitude is enhanced in gas at the solid particles that causes local generation of charges. The charge movement and accumulation causes a local potential to be seen by the primary single channel discharge and the ionizing front is split into multiple channels. This can be seen clearly with the iso-surface plot of electron density in Figure 5.5. The splitting of streamer channel also has an influence in propagating velocity, with speeds slower than the single channel propagation. The bridging of gap by streamer branches in Electric field iso-surfaces can be seen in Figure 5.6 and 5.7. It is important to stress here that the inhomogeneities needs to be located close to the streamer channel to split it, as being placed far away, solid particles has little influence on local electric field distribution.

(a)

(b)

(c)
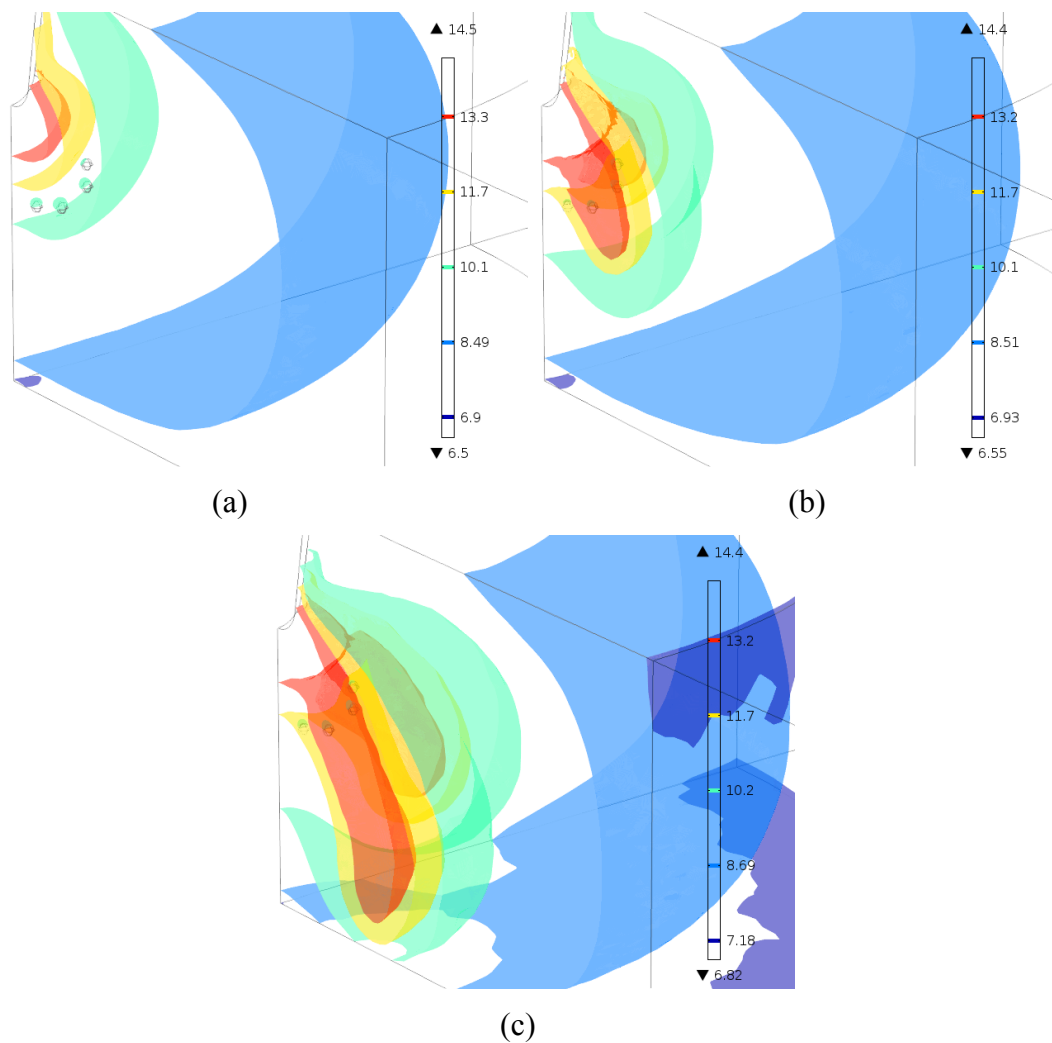
Figure 5.5 : Log of Electron density(cm^{-3}) plotted at (a) 1 ns (b) 3 ns (c) 6.4 ns
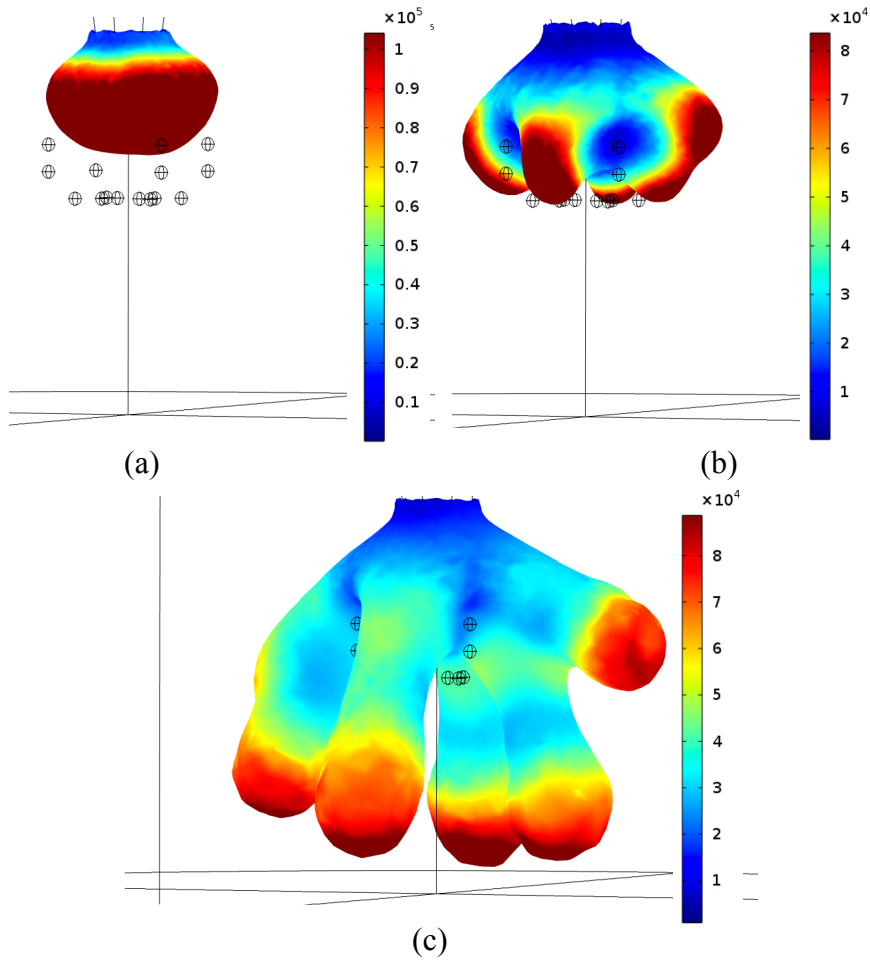
Figure 5.6: Electric field plot (V/cm) at (a) 1 ns (b) 3 ns (c) 6.4 ns

It is notable that results of simulations of streamer branching are sensitive to errors in the simulation model. Thus, it was observed that with a small streamer head and, correspondingly, smaller photoionization region in front of the streamer, the splitting of channel or detour is seen even without inclusion of charge accumulation centers if the mesh is not refined enough to resolve the head. Hence, the adaptive mesh refinement strategy is extremely important for efficient modeling.

Chapter 5 Simulation of streamer and streamer branching in 3d domain

6   Conclusion

An efficient computational framework has been developed to analyze charged species transport in air influenced by strong electric fields. The developed model is a set of coupled non-linear partial differential equations comprising: time dependent drift-diffusion equations for fluxes of charge carriers yielding dynamics of space charges, Poisson's equation for electric potential allowing for obtaining electric field distributions in gas volume affected by space charges, and three Helmholtz equations for calculating non-local photoionization rate. The model has been implemented in Comsol Multiphysics. The reactions rate coefficients for the drift-diffusion equations have been derived by numerical solution of Boltzmann equation for electrons energy distribution function in $N_2:O_2$ (80:20) mixture after introducing two-term approximation. To facilitate solution of transport equations, they were transformed into logarithmic form and were numerically stabilized using various test functions for weak finite element formulation. To increase the efficiency of the calculations and to reduce computational time, adaptive mesh refinement has been introduced into the model. Such developed computational framework has been utilized for several study cases to simulate development of streamer discharges in air in different 2d geometrical arrangements as well as to model streamer branching in fully 3d representation. The model of branching is introduced through inhomogeneities in gas modeled as solid particles. Charge accumulation on solid surfaces inherently leads to local field enhancements initiating splitting of streamer channel and formation of branches. The model is carefully checked against non-physical artefacts and numerical instabilities to avoid non-physical reasons for streamer branching. The efficiency of the numerical model allows to run fully 3d calculations with differently resolved domains within acceptable time.

Chapter 6 Conclusion

7   Future Work

Non-thermal discharges in air were studied in the present project utilizing the developed computational framework. The simulations were performed for streamer discharges in different 2d geometries and later more complicated 3d model of streamer branching was introduced. The next step planned is to consider discharges in air in the presence of solid elements in the form of insulating dielectric barriers. To mimic real situations, the barriers are to be floating and not in contact with metallic electrodes. A consistent physical model of such hybrid gas-solid system requires considering charge transport mechanisms on gas-solid interfaces as well as bulk conduction through the solid material. It is expected that implementation of these processes will increase the complexity of the problem considerably and, thus, introducing new methods to enhance the efficiency of the developed framework is highly desirable. Simulations of discharges in gas-solid insulation are expected to bring new knowledge needed for development and design of hybrid HV insulation systems, in particular, environmentally friendly SF_6-free insulation.

Chapter 7 Future work

8   References

[1]   E. Kuffel, W. S. Zaengl, and J. Kuffel, *High voltage engineering : Fundamentals*, 2nd ed. Oxford ; Boston: Butterworth-Heinemann, 2000.

[2]   J. J. Lowke and R. Morrow, "Theory of Electric-Corona Including the Role of Plasma Chemistry," *Pure and Applied Chemistry,* vol. 66, pp. 1287-1294, 1994.

[3]   N. L. Aleksandrov and E. M. Bazelyan, "Simulation of long-streamer propagation in air at atmospheric pressure," *Journal of Physics D: Applied Physics,* vol. 29, pp. 740-752, Mar 14 1996.

[4]   M. S. Benilov and G. V. Naidis, "Modelling of low-current discharges in atmospheric-pressure air taking account of non-equilibrium effects," *Journal of Physics D: Applied Physics,* vol. 36, pp. 1834-1841, Aug 7 2003.

[5]   A. Haddad and D. F. Warne, *Advances in high voltage engineering*. London: Institution of Electrical Engineers, 2004.

[6]   F. Grangé, J. Loiseau, and N. Spyrou, "Random distribution of background charge density for numerical simulation of discharge inception," *International Symposium on High Pressure Low Temperature Plasma Chemistry, HAKONE V,* 1996.

[7]   S. Pancheshnyi, "Role of electronegative gas admixtures in streamer start, propagation and branching phenomena," *Plasma Sources Science and Technology,* vol. 14, 2005.

[8]   W. S. Zaengl and K. Petcharaks, "Application of Streamer Breakdown Criterion for Inhomogeneous Fields in Dry Air and SF6," in *Gaseous Dielectrics VII*, ed: Springer US, 1994, pp. 153-159.

[9]   M. Ramesh, R. Summer, S. Singh, Y. V. Serdyuk, S. Gubanski, and S. Kumara, "Application of streamer criteria for calculations of flashover voltages of gaseous insulation with solid dielectric barrier," *Proceedings of 18th International Symposium on High Voltage Engineering,* pp. 1258-1263, Aug. 25-30 2013.

[10]   H. M. Ryan, D. Lightle, and D. Milne, "Factors Influencing Dielectric Performance of SF6 Insulated GIS," *IEEE transactions on Power Apparatus and Systems,* vol. PAS-104, pp. 1526-1535, 1985.

[11]   A. Starikovskiy, A. Nikipelov, and A. Rakitin, "Streamer Breakdown Development in Undercritical Electric Field," *IEEE Transactions on Plasma Science,* vol. 39, pp. 2606-2607, 2011.

[12]   Y. V. Serdyuk, "Propagation of Cathode-Directed Streamer Discharges in Air," *Proceedings of the COMSOL Conference , Rotterdam,* 2013.

[13]   Y. V. Serdyuk, *Numerical simulations of non-thermal electrical discharges in air*: Lightning electromagnetics , IET power and energy series, 2012, pp. 87-138.

[14]   E. Worts and S. D. Kovaleski, "Theoretical Investigation of a UV Laser Triggered Spark Gap," in *Pulsed Power Conference, IEEE*, 2005, pp. 623-626.

References

[15]   C. Thoma, D. R. Welch, D. V. Rose, W. R. Zimmerman, C. L. Miller, R. E. Clark*, et al.*, "Fully kinetic particle-in-cell simulations of triggered three-electrode gas switches," in *19th IEEE Pulsed Power Conference*, 2013, pp. 1-6.

[16]   M. Chung and E. Kunhardt, "Monte Carlo simulation of streamer propagation with E-E and E-E-ion collision," in *30th International Conference on Plasma Science*, 2003.

[17]   C. Li, J. Teunissen, M. Nool, W. Hundsdorfer, and U. Ebert, "A comparison of 3D particle, fluid and hybrid simulations for negative streamers," *Plasma Sources Science and Technology,* vol. 21, 2012.

[18]   B. V. Alexeev, *Generalized Boltzmann physical kinetics*, 1st ed.: Elsevier, 2004.

[19]   G. J. M. Hagelaar and L. C. Pitchford, "Solving the Boltzmann equation to obtain electron transport coefficients and rate coefficients for fluid models," *Plasma Sources Science and Technology,* vol. 14, pp. 722-733, 2005.

[20]   L. Pitchford and A. Phelps, "Comparative calculations of electron-swarm properties in N2 at moderate E/N values," *Physical Review A,* vol. 25, pp. 540-554, 1982.

[21]   A. Phelps and L. Pitchford, "Anisotropic scattering of electrons by N2 and its effect on electron transport," *Physical Review A,* vol. 31, pp. 2932-2949, 05/01/ 1985.

[22]   "COMSOL Plasma Module User Manual," vol. Version 4.4, 2013.

[23]   "Phelps database, http://www.lxcat.net, retrieved on January 10, 2013."

[24]   R. Morrow, "Properties of streamers and streamer channels in SF6," *Physical Review A,* vol. 35, pp. 1778-1785, 1987.

[25]   R. Morrow, "Theory of negative corona in oxygen," *Physical Review A,* vol. 32, pp. 1799-1809, 1985.

[26]   Y. V. Serdyuk, A. Larsson, S. M. Gubanski, and M. Akyuz, "The propagation of positive streamers in a weak and uniform background electric field," *Journal of physics D: applied physics.,* vol. 34, pp. 614-623, 2001.

[27]   Y. V. Serdyuk, "Computer Modelling of Electrophysical Phenomena in High Voltage Insulation," *Phd Thesis - Chalmers university of technology,* 2004.

[28]   Y. V. Serdyuk, S. M. Gubanski, J. Blennow, and M. Sjoberg, "Electrical discharge in an air gap with dielectric-covered electrodes," *Conference on Electrical Insulation and Dielectric Phenomena,* vol. 1, pp. 397-400, 2000.

[29]   R. Morrow and J. J. Lowke, "Streamer propagation in air," *Journal of Physics D: Applied Physics,* vol. 30, 1997.

[30]   G. E. Georghiou, A. P. Papadakis, R. Morrow, and A. C. Metaxas, "Numerical modelling of atmospheric pressure gas discharges leading to plasma production," *Journal of Physics D: Applied Physics,* vol. 38, pp. R303-R328, 2005.

[31]   A. Salabas, G. Gousset, and L. L. Alves, *Plasma Sources Science and Technology,* vol. 11, 2002.

[32]   A. A. Kulikovsky, "The role of photoionization in positive streamer dynamics," *Journal of Physics D: Applied Physics,* vol. 33, pp. 1514-1524, 2000.

[33]   A. Luque, U. Ebert, C. Montijn, and W. Hundsdorfer, "Photoionization in negative streamers: Fast computations and two propagation modes," *Applied Physics Letters,* vol. 90, 2007.

[34]   A. Bourdon, V. P. Pasko, N. Y. Liu, S. Célestin, P. Ségur, and E. Marode, "Efficient models for photoionization produced by non-thermal gas discharges in air based on radiative transfer and the Helmholtz equations," *Plasma Sources Science and Technology,* vol. 16, pp. 656-678, 2007.

[35]   G. Wormeester, S. Pancheshnyi, A. Luque, S. Nijdam, and U. Ebert, "Probing photo-ionization: simulations of positive streamers in varying N2 : O2-mixtures," *Journal of Physics D: Applied Physics,* vol. 43, p. 505201, 2010.

[36]   M. B. Zhelezniak, A. K. Mnatsakanian, and S. V. Sizykh, "Photoionization of nitrogen and oxygen mixtures by radiation from gas discharge," *High Temperature,* vol. 20, pp. 357–362, 1982.

[37]   A. A. Kulikovsky, "Reply to comment on 'The role of photoionization in positive streamer dynamics'," *Journal of Physics D: Applied Physics,* vol. 34, pp. 251-252, 2001.

[38]   S. V. Pancheshnyi and A. Y. Starikovskii, "Comments on 'The role of photoionization in positive streamer dynamics'," *Journal of Physics D: Applied Physics,* vol. 34, pp. 248-250, Jan 21 2001.

[39]   N. Liu, S. b. Célestin, A. Bourdon, V. P. Pasko, P. Ségur, and E. Marode, "Application of photoionization models based on radiative transfer and the Helmholtz equations to studies of streamers in weak electric fields," *Applied Physics Letters,* vol. 91, 2007.

[40]   P. Ségur, A. Bourdon, E. Marode, D. Bessieres, and J. H. Paillol, "The use of an improved Eddington approximation to facilitate the calculation of photoionization in streamer discharges," *Plasma Sources Science and Technology,* vol. 15, pp. 648-660, 2006.

[41]   C. Johnson, *Numerical solution of partial differential equations by the finite element method*: Dover Publications, 2009.

[42]   C. Montijn, W. Hundsdorfer, and U. Ebert, "An adaptive grid refinement strategy for the simulation of negative streamers," *Journal of Computational Physics,* vol. 219, pp. 801-835, 2006.

[43]   "COMSOL Multiphysics User Manual," vol. Version 4.4, 2013.

[44]   S. V. Patankar, *Numerical heat transfer and fluid flow*, 1980.

[45]   A. P. Papadakis, G. E. Georghiou, and A. C. Metaxas, "Two-dimensional axisymmetric simulations and the heating effects associated with DC atmospheric pressure discharges during the post-streamer stage," *IET Science, Measurement & Technology,* vol. 1, pp. 113-120, 2007.

[46]   S. Singh, "Adaptive Numerical Simulation of Streamer Propagation in Atmospheric Air," *Proceedings of the COMSOL Conference in Rotterdam,* 2013.

[47]   G. E. Georghiou, R. Morrow, and A. C. Metaxas, "A two-dimensional, finite-element, flux-corrected transport algorithm for the solution of gas discharge problems," *Journal of Physics D: Applied Physics,* vol. 33, pp. 2453-2466, 2000.

[48]   G. E. Georghiou, R. Morrow, and A. C. Metaxas, "Two-dimensional simulation of streamers using the FE-FCT algorithm," *Journal of Physics D: Applied Physics,* vol. 33, pp. L27-L32, 2000.

References

[49]   A. Luque, U. Ebert, C. Montijn, and W. Hundsdorfer, "Streamers in 3d Photoionization and streamer interaction," *Workshop on streamers, sprites, leaders, lightining: from micro to macro scales,* Leiden, Oct 8-12 2007.

[50]   A. Starikovskiy, "Fast Ionization Wave Development in Atmospheric-Pressure Air," *IEEE Transactions on Plasma Science,* vol. 39, pp. 2602-2603, 2011.

[51]   E. Panousis, L. Papageorghiou, N. Spyrou, J. F. Loiseau, B. Held, and F. Clément, "Numerical modelling of an atmospheric pressure dielectric barrier discharge in nitrogen: electrical and kinetic description," *Journal of Physics D: Applied Physics,* vol. 40, pp. 4168-4180, 2007.

[52]   E. M. van Veldhuizen, P. C. M. Kemps, and W. R. Rutgers, "Streamer branching in a short gap: The influence of the power supply," *IEEE Transactions on Plasma Science,* vol. 30, pp. 162-163, 2002.

[53]   A. Luque and U. Ebert, "Electron density fluctuations accelerate the branching of positive streamer discharges in air," *Physical Review E,* vol. 84, 2011.

[54]   M. Akyuz, A. Larsson, V. Cooray, and G. Strandberg, "3D simulations of streamer branching in air," *Journal of Electrostatics,* vol. 59, pp. 115-141, 2003.

[55]   A. Rocco, U. Ebert, and W. Hundsdorfer, "Branching of negative streamers in free flight," *Physical Review E,* vol. 66, 2002.

[56]   J. Jadidian, M. Zahn, N. Lavesson, O. Widlund, and K. Borg, "Stochastic and deterministic causes of streamer branching in liquid dielectrics," *Journal of Applied Physics,* vol. 114, 2013.

[57]   A. A. Kulikovsky, "Comment on ``Spontaneous Branching of Anode-Directed Streamers between Planar Electrodes"," *Physical Review Letters,* vol. 89, 2002.

[58]   A. L. Kupershtokh and D. I. Karpov, "Simulation of the development of branching streamer structures in dielectric liquids with pulsed conductivity of channels," *Technical Physics Letters,* vol. 32, pp. 406-409, 2006.